



Mechanistic insights into novel cyano-pyrimidine pendant chalcone derivatives as LSD1 inhibitors by docking, ADMET, MM/GBSA, and molecular dynamics simulation

Amisha Gupta^a, Darakhshan Parveen^a, Faizul Azam^b, M. Shaquiquzzaman^{a,*},
Mymoona Akhter^a, Mariusz Jaremko^c, Abdul-Hamid Emwas^c, Mohammad Ahmed Khan^d,
Suhel Parvez^e, Suruchi Khanna^d, Rituparna Palit^f, Umar Jahangir^g, M. Mumtaz Alam^{a,*} 

^a Drug Design and Medicinal Chemistry Lab, Department of Pharmaceutical Chemistry, School of Pharmaceutical Education & Research, Jamia Hamdard, New Delhi, 110062, India

^b Department of Medicinal Chemistry and Pharmacognosy, College of Pharmacy, Qassim University, Buraydah, 51452, Saudi Arabia

^c King Abdullah University of Science and Technology (KAUST), 23955-6900, Thuwal, Kingdom of Saudi Arabia

^d Department of Pharmacology, School of Pharmaceutical Education & Research, Jamia Hamdard, New Delhi, 110062, India

^e Department of Toxicology, School of Chemical and Life Sciences, Jamia Hamdard, New Delhi, 62, India

^f Department of Pharmaceutical Chemistry, RKGIT, AKTU, Uttar Pradesh, India

^g Department of Amraz-e-Jild, School of Unani Medical Education and Research, Jamia Hamdard, New Delhi, 110062, India

ARTICLE INFO

Keywords:

Cancer
LSD1
Chalcone
Cyano-pyrimidine
Molecular docking
Molecular dynamics

ABSTRACT

Cancer presents a formidable and complex foe, standing as one of the foremost contributors to disease-related fatalities across the globe. According to data from the Global Cancer Observatory (GLOBOCAN), projections indicate a staggering 28.4 million cases of cancer, encompassing both new diagnoses and deaths, by 2040. Therefore, developing effective and comprehensive treatment approaches for cancer patients is essential and the conventional approved treatments for cancers are associated with various harmful side effects. Our study aims to address the critical and widespread need for alternative therapies that can effectively combat cancer with minimal side effects.

The present contribution outlines a targeted approach using Lysine Specific Demethylase 1 (LSD1) to evaluate novel cyano-pyrimidine pendant chalcone derivatives as potential antiproliferative agents. Two sets of novel cyano-pyrimidine pendant chalcone derivatives were produced, and molecular docking was performed on the LSD1 protein. The ligands A1 and B1 belonging to series A and B, respectively, were found to have the highest docking scores of -11.095 and -10.773 kcal/mol, in that order. The ADME and toxicity studies of the ligands showed promising responses with respect to various pharmacokinetic and physicochemical parameters. The Molecular dynamics (MD) simulation results indicated effective diffusion of both complexes inside the protein cavity, facilitated by prominent interactions with various amino acids. Additionally, the complexes displayed high relative binding free energy. The computational screening of ligands indicates that ligands A1 and B1 exhibit potential for further exploration using various *in vitro* and *in vivo* techniques. These ligands may then serve as promising leads in the discovery of cancer drugs. The *in-silico* screening of the novel library of cyano-pyrimidine pendant chalcone derivatives was performed with a combination of molecular docking, MM-GBSA, ADME, toxicity and MD simulation. Molecular docking and MM-GBSA were conducted using the Glide and Prime tools, respectively, of the Schrödinger suite 12.8. The ligands were analysed for ADME using the Swiss ADME, while toxicity risks were evaluated using Osiris Property Explorer. Additionally, a 400ns MD simulation

* Corresponding author. Drug Design and Medicinal Chemistry Lab, Department of Pharmaceutical Chemistry, School of Pharmaceutical Education and Research, Jamia Hamdard, New Delhi, 110062, India.

** Corresponding author. Drug Design and Medicinal Chemistry Lab, Department of Pharmaceutical Chemistry, School of Pharmaceutical Education and Research, Jamia Hamdard, New Delhi, 110062, India.

E-mail addresses: shaqiq@gmail.com (M. Shaquiquzzaman), drmmalam@gmail.com, mmalam@jamiyahamdard.ac.in (M.M. Alam).

<https://doi.org/10.1016/j.bbrep.2025.101937>

Received 1 December 2024; Received in revised form 15 January 2025; Accepted 26 January 2025

2405-5808/© 2025 The Author(s). Published by Elsevier B.V. This is an open access article under the CC BY-NC-ND license (<http://creativecommons.org/licenses/by-nc-nd/4.0/>).

of LIGA1 and LIGB1 against the protein LSD1 was performed using the Desmond tool of Schrödinger suite 12.8 to validate the docking results and analyse the behaviour and stability of the complexes.

1. Introduction

Over the years, the focus of cancer therapy has evolved from traditional treatments such as chemotherapy and radiation, to the role of epigenetics in cancer development and progression. Researchers are investigating how the modification of gene expression, without altering the underlying DNA sequence, can be targeted for therapeutic purposes. In this regard, the discovery of novel epigenetic regulators has created opportunities for potential cancer treatments, while ongoing research into various pharmaceuticals for cancer therapy remains of high importance to assess the efficacy of these anticancer agents for treatment [1]. In late 2004, Yang Shi and colleagues [2] discovered the potential epigenetic target for cancer therapy, *i.e.*, the Lysine Specific Demethylase 1 (LSD1) [3]. The initial discovery of LSD1 revealed that this is a nucleoprotein with an affinity for flavin adenine dinucleotide (FAD) sharing sequence homology with FAD-dependent amine oxidases [4]. LSD1, also referred to as KDM1A, AOF2, and BHC110 [5] regulates the cell differentiation. Its dysregulation is closely linked to carcinogenesis [6] via its ability to remove the methyl groups from mono- or di-methylated lysine residues of histone [H3 lysine 4 (H3K4) and H3K9] and non-histone proteins [7–8]. The underlying mechanistic pathway involves the oxidation of the methyl group of a substrate like H3K4–Me1 or 2 by FAD, forming an imine intermediate. Subsequent hydrolysis generates demethylated products along with formaldehyde [9]. This catalytic cycle is completed by the subsequent oxidation of the

remaining reduced FAD by molecular oxygen [10].

The various forms of cancer have been found to exhibit aberrant expression of LSD1 [11] while downregulation of LSD1 expression through RNA interference (siRNA) or inhibition using small molecules has shown potential for preventing the proliferation of cancerous cells [12]. In particular, poorly differentiated neuroblastoma, neuroendocrine carcinomas, sarcoma, breast cancer, bladder cancer, lung cancer, gastric cancer, colon cancer, and ovarian cancer cells have all been found to express high levels of LSD1 proteins [13–18]. Thus, substantial evidence supports the pivotal role of LSD1 in the initiation and progression of cancer, prompting the exploration of LSD1 as a therapeutic target for cancer treatment. Several LSD1 inhibitors have been documented in the literature and are currently undergoing clinical trials. These include Vafidemstat [17], Iadademstat [19], Tranylcypromine [20], SP-2509 [21], GSK2879552 [22], CC-90011 [23] and OG-L002 [24]. The chemical structures of these inhibitors are shown in Fig. 1.

The inhibition of LSD1 holds significant importance then in the fight against cancer, a leading cause of mortality second only to cardiovascular disease [25]. Its pervasive presence continues to impact and claim millions of lives daily, necessitating urgent and effective interventions. An exhaustive literature review has identified the pyrimidine nucleus as a widely utilized structure for developing safe and effective LSD1 inhibitors for cancer treatment [26]. The nucleus is a key component present in various FDA-approved anticancer drugs like 5-Fluorouracil

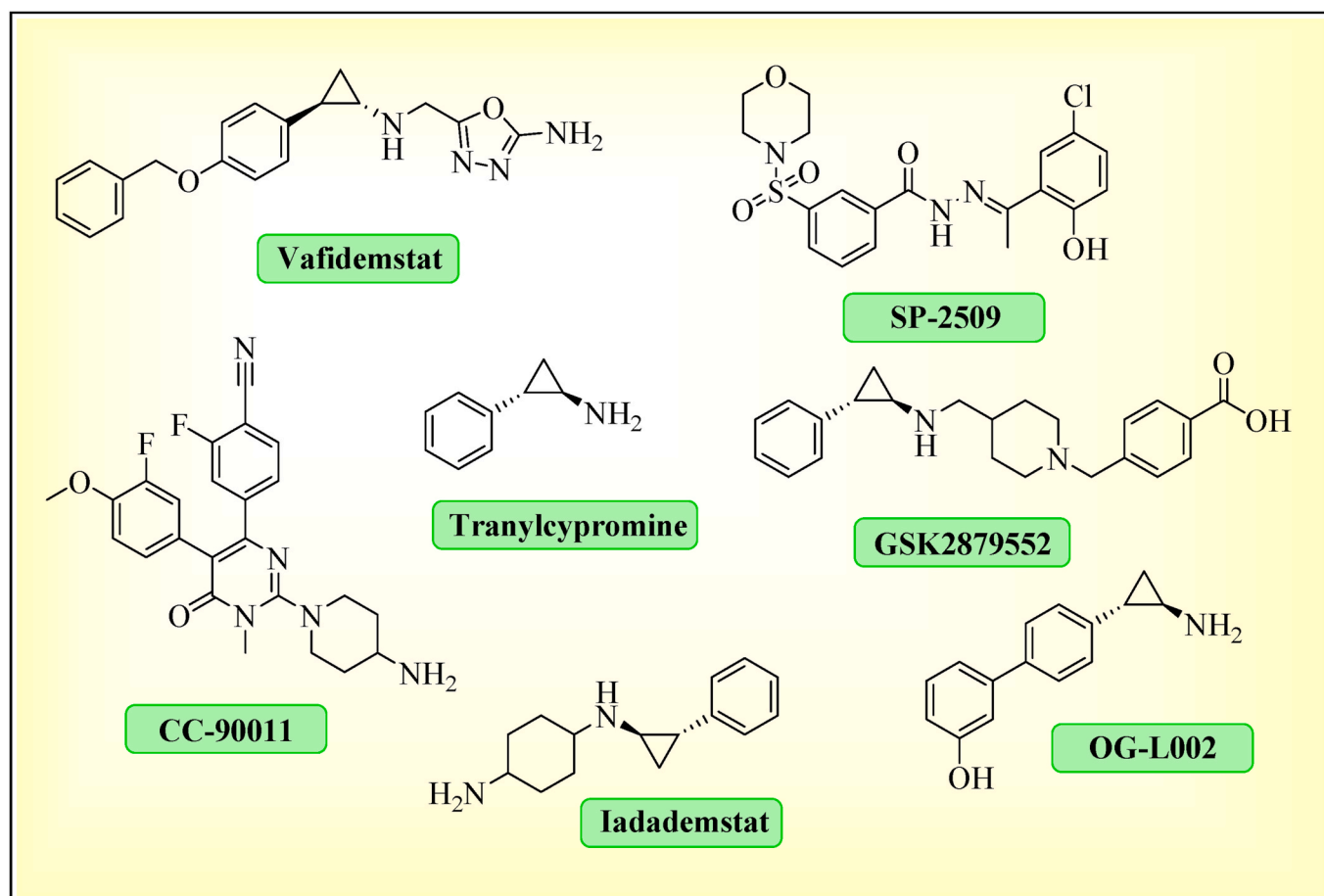


Fig. 1. LSD1 inhibitors in clinical trails.

[27], Bringatinib [28], Ceritinib (LDK378) [29], Dasatinib [30], Imatinib [31], Ibrutinib (IBR) [32], Merbarone [33], Nilotinib [34], Ruxolitinib (INC424) [35], Ribociclib [36] and Methotrexate [37]. While no LSD-1 inhibitor has been approved by the FDA to date, many experimental drugs with a pyrimidine core have demonstrated excellent results as LSD-1 inhibitors in pre-clinical studies of potential cancer treatment agents. For example, Li et al. synthesized several triazole-fused pyrimidine derivatives, with the most potent one exhibiting an IC_{50} value of 49 nM against LSD1 [38]. Metwally et al. [39] developed a series of pyrazolo [1,5-*a*]pyrimidines with the most effective compound displaying an IC_{50} value of 1.91 μ M. Wang et al. synthesized a series of triazolo [1,5-*a*]pyrimidine-based LSD1 inhibitors, with the most potent compound demonstrating reversible inhibition of LSD1 with an IC_{50} of 1.72 μ M [40]. The novel 5-arylidene barbiturates were explored by Xu et al., which exhibited reversible LSD1 inhibition with IC_{50} of 0.41 μ M [41]. Ma et al. reported on 5-cyano-6-phenylpyrimidine derivatives, with the most active compound repressing LSD1 with an IC_{50} value of 183 nM [42]. In sum, the collective body of research underscores the potential of pyrimidine derivatives as potent anticancer agents.

In addition to pyrimidines, chalcone has been explored by various researchers for treatment of cancer [43]. A literature survey suggests that chalcones can cause cell-cycle disruption and apoptosis [44], inhibit tubulin polymerization [45] and also inhibit kinases that are essential for the cancer cell survival and proliferation [46]. Furthermore, several chalcone-based FDA-approved anticancer medications are available in the market, such as Butein [47], Xanthohumol [48], Isoliquiritigenin [49] and Licochalcone A [50] etc. Ngameni et al. synthesized a new series of *o*-substituted chalcone derivatives with an/a allyl-, prenyl- or

propargyl-substituent at different positions [51]. Most of their novel synthesized compounds had IC_{50} values less than 1 μ M against several cell lines such as HCT116 p53 colon adenocarcinoma cells, CCRF-CEM cells, and MDA-MB-231-BCRP breast adenocarcinoma cells. In separate research conducted by Srilaxmi et al. a series of novel chalcone-linked pyrido [4,3-*b*] pyrazin-5(6*H*)-one derivatives were synthesized and evaluated for their anticancer activities against five human cancer cell lines such as MCF-7, A-549, colo-205, A2780 and DU-145. The IC_{50} values were in the range of 0.012–19.4 μ M [52].

Many researchers have suggested that the combination of pyrimidine and chalcone may be potent anticancer moieties. Wang et al. synthesized a series of [1,2,4] triazolo [1,5-*a*] pyrimidines bearing chalcone and found that one of the synthesized compounds inhibited the growth of PC-9 cells (IC_{50} = 0.59 μ M). This inhibition was approximately 4-fold more than 5-Fluorouracil [53]. Similarly, Bagul et al. developed chalcone-linked pyrazolo [1,5-*a*] pyrimidines and evaluated their anti-proliferative activity. Amongst these compounds, the IC_{50} of the most active compound was 2.6 μ M against the MDA-MB-231 cell line. Additionally, the compounds showed antiproliferative activity within the range of 2.6–34.9 μ M against lung cancer (A549), MDA-MB-231 (breast cancer), and prostate cancer (DU-145) cell lines [54]. The structures of FDA-approved drugs based on pyrimidine and chalcone nucleus are shown in Fig. 2.

Considering the importance of the pharmacophoric scaffolds (pyrimidine and chalcone) alone or in combination, the basic moiety was designed by conjugating these moieties with specific modifications to achieve the desired properties. For example, the pyrimidine ring substituted with a sulphur-containing isopropyl side chain and a nitrile group has been shown to exhibit anticancer properties [55]. The

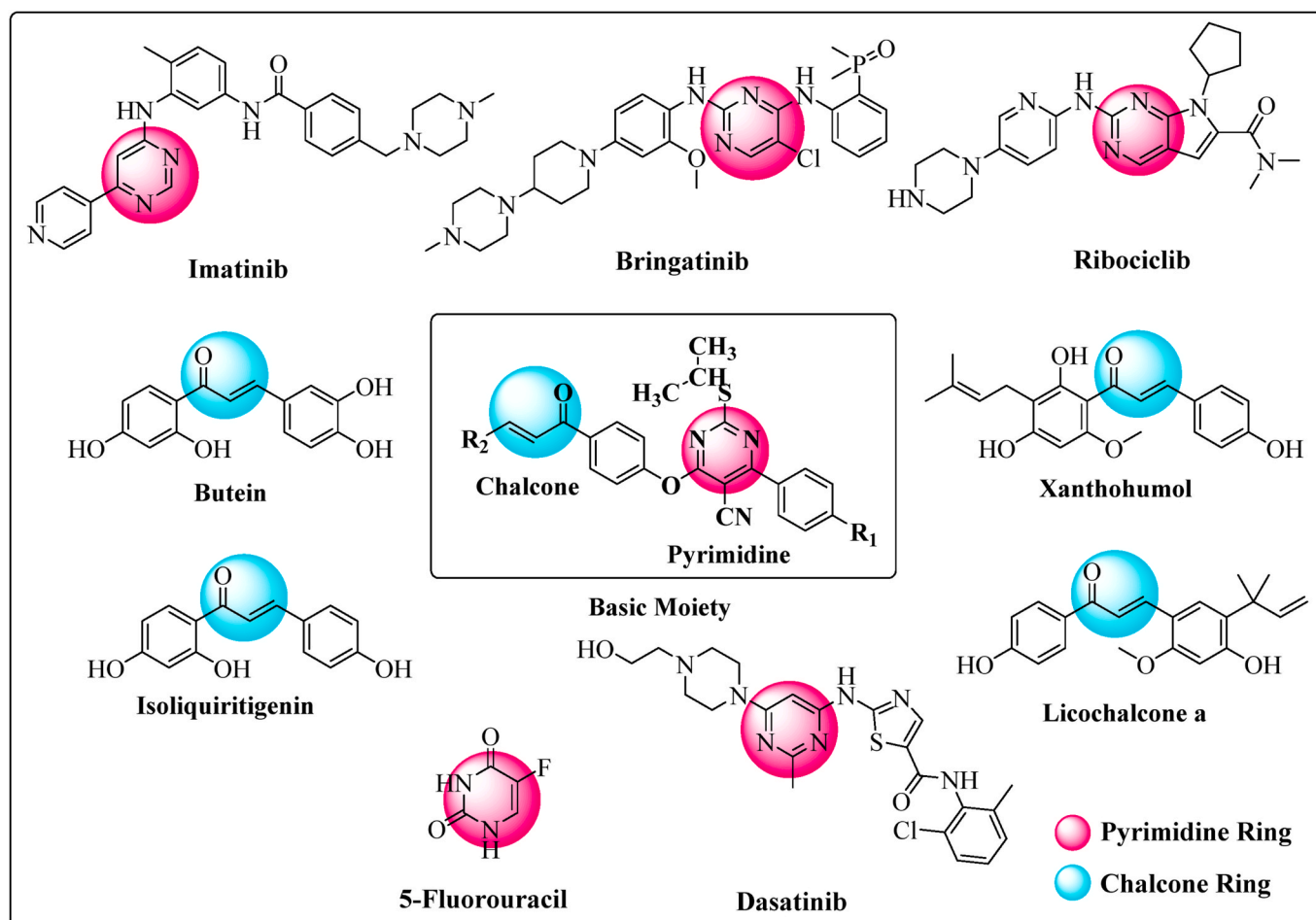


Fig. 2. Marketed drugs containing basic moiety constructs.

inclusion of sulphur [56] and nitrile functionalities [57] [58] helps to enhance the biocompatibility of the candidate drug in the body. Additionally, lipophilic alkyl side chains significantly enhance the potency of the anticancer molecules by improving their affinity for cell membranes and, hence, enhance their permeability [59]. Thus, substituting the sulphur atom with the isopropyl side chain was a deliberate choice.

The aim of the study reported in this paper was to develop a novel cyano-pyrimidine pendant chalcone conjugate demonstrating enhanced anticancer activity compared to the individual efficacy of each constituent moiety. For this purpose, a library comprising 3688 novel cyano-pyrimidine pendant chalcone conjugates was designed through multiple enumerations using Schrödinger's Prime Version 12.8. These conjugates were then studied further using computational tools like molecular docking, ADMET, MMGBSA and Molecular dynamics (MD) simulation targeting LSD1.

2. Materials and methods

2.1. Library creation

The chemical structures of series A and B of cyano-pyrimidine pendant chalcone derivatives were designed using ChemDraw 21.0.0. Subsequently, their derivatization was carried out using the enumeration tool of Schrödinger suite 12.8. The novelty of all the prepared compounds was validated using SciFinder.

2.2. Molecular docking

The X-ray crystal structure of LSD1 protein (PDB ID: 2DW4) was obtained from the RCSB Protein Data Bank. The protein preparation wizard and ligand preparation module of Schrödinger suite 12.8 were used to prepare protein and test ligands, respectively. Molecular docking was done on the Glide tool of Schrödinger Maestro Version 12.8 using high-throughput virtual screening (HTVS) mode [60].

The Ligprep module was used to prepare test ligands using the default settings for the OPLS4 force field, generating a maximum of 32 conformers per ligand. The LSD1 protein (PDB ID: 2DW4) was imported from the protein preparation wizard and then preprocessed. Thereafter, water molecules, additional undesirable side chains, residues and heteroatoms of the protein were removed, and appropriate bond orders were assigned. The protein was optimized and minimized using the OPLS4 force field. Following protein preparation, the receptor grid was created using the default settings of the receptor grid generation tool of Schrödinger by selecting a portion of the protein chain.

Ligand docking was performed by importing the grid files and preparing ligands in HTVS mode. Then, the docking results were exported and analysed.

2.3. MM-GBSA analysis

The MM-GBSA analysis was performed using the Prime tool of Schrödinger suite 12.8 [61]. The ligands with the highest docking score within the range of -11 kcal/mol to -10 kcal/mol from both series were further analysed for MM-GBSA (using the forcefield OPLS4 and VSGB solvation model) to calculate the binding free energies of the docking complex. The binding free energies of the receptor-ligand complex obtained from MM-GBSA were utilized to validate the docking results further and optimize the candidate ligands.

2.4. Estimation of ADME properties and toxicity risks

Following docking analysis, the screened compounds were evaluated using the SwissADME [62] software. This tool examines critical pharmacological attributes such as lipophilicity, water solubility, pharmacokinetics, drug-likeness, bioavailability and many other chemical characteristics essential for drug discovery. The compound's SMILES

structures were submitted to the server to obtain all relevant ADME attributes. Osiris Property Explorer was also utilized to analyse the screened compounds for reproductive toxicity, mutagenicity, tumorigenicity, and irritancy [63].

2.5. MD simulation

The MD simulation study was done to validate the molecular docking [64], assess the conformational stability and analyse the thermodynamic behaviour of the top-scoring protein-test ligand complexes from both series' (2DW4-A1 and 2DW4-B1) complexes. The study was performed using the Desmond tool of Schrödinger suite 12.8 [65]. The simulations ran for 400 ns at the constant temperature of 300 K and pressure of 1.01325 bar. The temperature was regulated using the Nose-Hoover thermostat, and the pressure was controlled using the Martyna-Tobias-Klein method. Before the simulations, the system underwent minimization and equilibration procedures following Desmond's default methods. The complexes were analysed using a protein-ligand contact plot, simulation quality plot, RMSF and RMSD. They were placed in an orthorhombic box of 10 Å periodic boundary with explicit water molecules using a simple point charge (SPC) water model. The force field OPLS3e was applied, a 0.15 M salt solution was used to neutralize the system, while the Na^+ and Cl^- ions simulated the physiological conditions. Vanderwaal and Coulomb interactions were analysed with a cut-off radius of 9.0 Å; the Particle Mesh Ewald method was used for electrostatic interactions evaluation. The trajectory files were assessed using simulation event, quality and interaction diagram protocols, while the equations of motion were analysed using a reference system propagator algorithm [66].

3. Results and discussion

3.1. Library creation

Using the enumeration module of Schrödinger suite 12.8, a comprehensive library consisting of 3668 test ligands was generated, with 1834 ligands each allocated to the A and B series. Subsequently, using Ligprep of Schrödinger suite 12.8, 6160 test ligands, with 3080 ligands attributed to each series A and B, were generated. Finally, all prepared ligands were docked against the prepared LSD1 protein (PDB ID: 2DW4).

3.2. Molecular docking

The docking of all the ligands was done on the binding pocket of the LSD1 protein where the native ligand FAD was bound. Iadademstat, Vafidemstat, 5-Fluorouracil, Xanthohumol and Dasatinib were used as reference standards to determine the test ligand's efficacy. The docking results showed that all the ligands fit well within the protein's active site. Notably, most of the enumerated ligands of both series A and B showed superior binding affinity compared to the reference drugs, with binding affinities of -8.129 , -6.836 , -6.431 , -5.722 and -5.007 kcal/mol for Iadademstat, Vafidemstat, 5-Fluorouracil, Xanthohumol and Dasatinib, respectively. Among both series A and B, the test ligands A1 and B1 showed the highest binding affinity with docking scores of -11.095 and -10.773 kcal/mol, respectively. The higher binding affinity of the test drugs may be due to the greater number of hydrogen bonds and interactions compared to the reference drugs. The 2D and 3D binding interactions of ligands A1 and B1 were analysed and are depicted in the figures, Figs. 3 and 4. The analysis of 2D interactions showed that test ligand A1 formed two hydrogen bonds with ASP556 and GLU559, a salt bridge with GLU559, and π - π stacking with TYR761. Ligand B1 formed three hydrogen bonds with ARG316, TRP756 and ARG310 and π - π stacking with TYR761.

The various reference drugs showed various similar and dissimilar interactions with the protein. The reference drug Iadademstat displayed

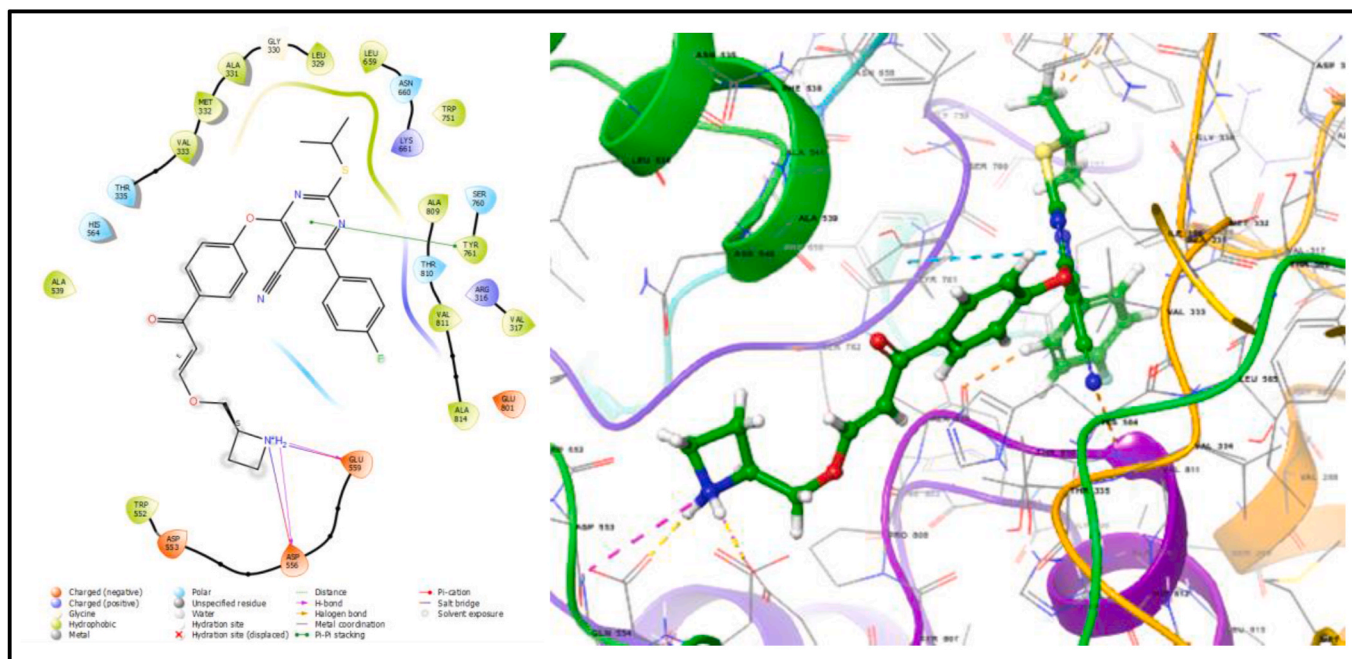


Fig. 3. 2D and 3D binding interactions of ligand A1 and the 2DW4 complex.

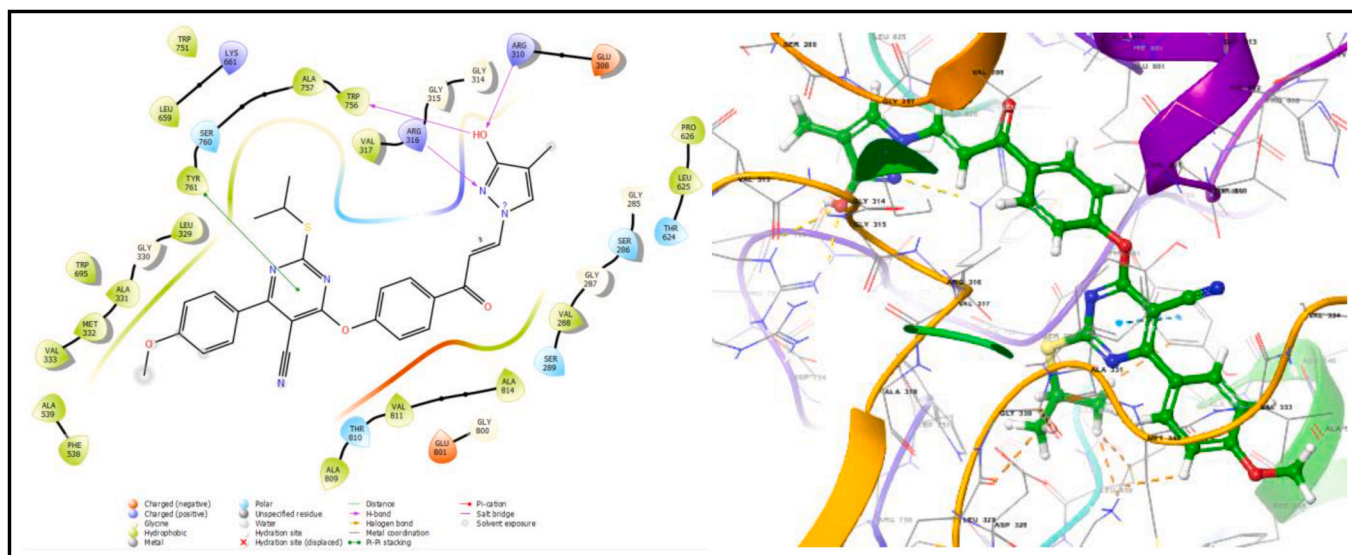


Fig. 4. 2D and 3D binding interactions of ligand B1 and the 2DW4 complex.

only one hydrogen bond with amino acid LEU329, Vafidemstat showed four interactions among which three were hydrogen bonds with SER289, THR624 and THR810, and one π - π stacking with TYR761. Another reference drug Xanthohumol showed two interactions: one hydrogen bond, and one π - π stacking with VAL288 and TYR761, respectively, whereas Dasatinib had one π - π stacking with TYR761 and one π -cation bond with ARG316. The reference drug 5-Fluorouracil had three interactions: hydrogen bond with SER289, salt bridge and π - π stacking with ARG316.

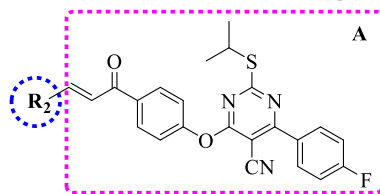
The π - π stacking bond with TYR761 of our compounds with highest docking score from each series was similar to the reference standards Vafidemstat, Xanthohumol and Dasatinib.

Tables 1 and 2 report the enumerated R₂ groups of the top 25 test ligands of each series, A and B, along with their docking scores.

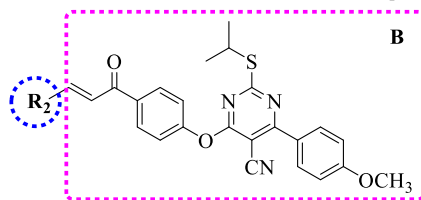
3.3. MM-GBSA analysis

From series A and B, the ligands with docking scores within the range of -11 to -10 kcal/mol were selected for Prime MM-GBSA analysis to compute the binding free energy of the ligand-receptor complex (Table 3). The study revealed the binding strength of the ligands with the receptor.

Within series A, ligand A16 showed the highest MM-GBSA binding energy, i.e., -95.85 kcal/mol, while within series B, ligand B18 had the highest binding free energy of -96.02 kcal/mol. Despite the ligands A1 and B1 possessing the highest docking scores within their respective series, they did not display the highest binding potential in MM-GBSA analysis (A1: -71.97 kcal/mol; B1: -91.03 kcal/mol). Nonetheless, in comparison to most ligands, ligands A1 and B1 demonstrated a favourable binding potential. Furthermore, the binding affinity of ligand

Table 1Docking scores of reference drugs and top 25 ligands of series A with their substitutions at the R₂ position.

| Ligand | R ₂ | Docking score | Ligand | R ₂ | Docking score |
|----------------|----------------|---------------|--------|----------------|---------------|
| Iadademstat | - | -8.129 | A11 | | -10.172 |
| Vafidemstat | - | -6.836 | A12 | | -10.134 |
| 5-Fluorouracil | - | -6.431 | A13 | | -10.113 |
| Xanthohumol | - | -5.722 | A14 | | -10.082 |
| Dasatinib | - | -5.007 | A15 | | -10.073 |
| A1 | | -11.095 | A16 | | -10.061 |
| A2 | | -11.08 | A17 | | -10.048 |
| A3 | | -10.363 | A18 | | -10.026 |
| A4 | | -10.346 | A19 | | -10.016 |
| A5 | | -10.323 | A20 | | -10.013 |
| A6 | | -10.320 | A21 | | -10.009 |
| A7 | | -10.289 | A22 | | -9.961 |
| A8 | | -10.286 | A23 | | -9.947 |
| A9 | | -10.275 | A24 | | -9.924 |
| A10 | | -10.220 | A25 | | -9.889 |

Table 2Docking scores of reference drugs and the top 25 ligands of series B with their substitutions at the R₂ position.

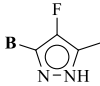
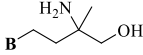
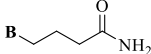
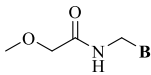
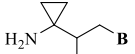
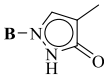
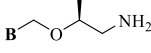
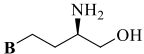
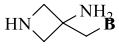
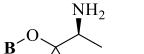
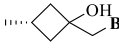
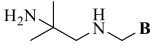
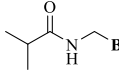

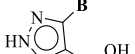
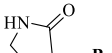
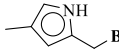
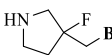
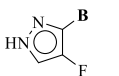
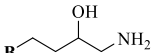

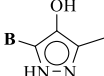

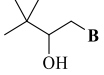
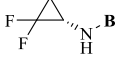
| Ligand | R ₂ | Docking score | Ligand | R ₂ | Docking score |
|----------------|---|---------------|--------|---|---------------|
| Iadademstat | - | -8.129 | B11 |  | -10.182 |
| Vafidemstat | - | -6.836 | B12 |  | -10.179 |
| 5-Fluorouracil | - | -6.431 | B13 |  | -10.168 |
| Xanthohumol | - | -5.722 | B14 |  | -10.137 |
| Dasatinib | - | -5.007 | B15 |  | -10.125 |
| B1 |  | -10.773 | B16 |  | -10.12 |
| B2 |  | -10.66 | B17 |  | -10.118 |
| B3 |  | -10.598 | B18 |  | -10.11 |
| B4 |  | -10.456 | B19 |  | -10.091 |
| B5 |  | -10.437 | B20 |  | -10.09 |
| B6 |  | -10.35 | B21 |  | -10.064 |
| B7 |  | -10.35 | B22 |  | -10.039 |
| B8 |  | -10.267 | B23 |  | -10.036 |
| B9 |  | -10.242 | B24 |  | -10.033 |
| B10 |  | -10.214 | B25 |  | -9.986 |

Table 3
Computed binding free energies (ΔG_{bind}) of selected ligands against LSD1.

| Ligand | Binding Energy (ΔG_{Bind}) | Ligand | Binding Energy (ΔG_{Bind}) | Ligand | Binding Energy (ΔG_{Bind}) |
|--------|---|--------|---|--------|---|
| A1 | -71.97 | A16 | -95.85 | B10 | -82.14 |
| A2 | -66.82 | A17 | -90.41 | B11 | -92.82 |
| A3 | -50.09 | A18 | -84.82 | B12 | -81.20 |
| A4 | -82.74 | A19 | -84.37 | B13 | -93.14 |
| A5 | -67.31 | A20 | -82.74 | B14 | -71.86 |
| A6 | -82.24 | A21 | -63.27 | B15 | -64.06 |
| A7 | -72.11 | B1 | -91.03 | B16 | -77.90 |
| A8 | -91.56 | B2 | -89.84 | B17 | -66.20 |
| A9 | -87.66 | B3 | -77.44 | B18 | -96.02 |
| A10 | -68.13 | B4 | -67.80 | B19 | -80.38 |
| A11 | -84.44 | B5 | -48.00 | B20 | -68.84 |
| A12 | -65.07 | B6 | -82.89 | B21 | -78.25 |
| A13 | -75.75 | B7 | -66.89 | B22 | -89.31 |
| A14 | -82.56 | B8 | -89.40 | B23 | -94.81 |
| A15 | -73.08 | B9 | -86.36 | B24 | -88.92 |

Table 4
Physicochemical properties of ligands with best 45 docking scores for targeting of LSD1.

| Lig. | Formula | Lipinski's rule of 5 | | | | Lipinski violations | FCsp ³ | RB | MR | TPSA (\AA^2) | HA | AHA |
|------|---|----------------------|------|------|-------|---------------------|-------------------|----|--------|-------------------------|----|-----|
| | | MW (g/mol) | HBA. | HBD. | MLogP | | | | | | | |
| A1 | C ₂₇ H ₂₅ FN ₄ O ₃ S | 504.58 | 8 | 1 | 2.31 | 1 | 0.26 | 10 | 139.44 | 122.43 | 36 | 18 |
| A2 | C ₂₉ H ₂₉ FN ₄ O ₂ S | 516.63 | 7 | 1 | 3.5 | 1 | 0.31 | 10 | 147.96 | 113.2 | 37 | 18 |
| A3 | C ₂₈ H ₂₈ FN ₅ O ₂ S | 517.62 | 8 | 2 | 2.5 | 1 | 0.29 | 9 | 145.86 | 139.22 | 37 | 18 |
| A4 | C ₂₇ H ₂₄ FN ₃ O ₃ S ₂ | 521.63 | 7 | 1 | 3.11 | 1 | 0.26 | 8 | 140.39 | 146.7 | 36 | 18 |
| A5 | C ₂₉ H ₂₉ FN ₄ O ₂ S | 516.63 | 7 | 1 | 3.5 | 1 | 0.31 | 10 | 143.69 | 127.19 | 37 | 18 |
| A6 | C ₂₆ H ₂₃ FN ₄ O ₄ S | 506.55 | 8 | 1 | 1.66 | 1 | 0.19 | 11 | 133.03 | 139.5 | 36 | 18 |
| A7 | C ₂₇ H ₂₈ FN ₅ O ₂ S | 505.61 | 8 | 2 | 2.31 | 1 | 0.26 | 11 | 139.26 | 139.22 | 36 | 18 |
| A8 | C ₂₇ H ₂₅ FN ₅ O ₃ S | 518.58 | 9 | 2 | 2.33 | 1 | 0.26 | 9 | 145.27 | 133.43 | 37 | 18 |
| A9 | C ₂₇ H ₂₄ FN ₅ O ₃ S | 517.57 | 8 | 1 | 2.67 | 1 | 0.22 | 9 | 145.36 | 133.51 | 37 | 18 |
| A10 | C ₂₈ H ₂₈ FN ₅ O ₂ S | 517.62 | 7 | 1 | 2.5 | 1 | 0.29 | 10 | 142.08 | 130.43 | 37 | 18 |
| A11 | C ₂₈ H ₂₉ FN ₄ O ₃ S | 520.62 | 8 | 2 | 2.5 | 1 | 0.29 | 10 | 142.46 | 147.42 | 37 | 18 |
| A12 | C ₂₈ H ₂₅ FN ₄ O ₃ S | 516.59 | 7 | 1 | 2.84 | 1 | 0.25 | 9 | 143.36 | 130.27 | 37 | 18 |
| A13 | C ₂₈ H ₂₇ FN ₄ O ₂ S | 502.6 | 7 | 1 | 3.3 | 1 | 0.29 | 9 | 143.16 | 113.2 | 36 | 18 |
| A14 | C ₂₈ H ₂₇ FN ₅ O ₂ S | 516.61 | 8 | 1 | 2.91 | 1 | 0.29 | 9 | 148.91 | 113.2 | 37 | 18 |
| A15 | C ₂₈ H ₃₀ FN ₅ O ₂ S | 519.63 | 8 | 1 | 2.5 | 1 | 0.29 | 11 | 144.16 | 130.43 | 37 | 18 |
| A16 | C ₂₇ H ₂₇ FN ₄ O ₃ S | 506.59 | 8 | 2 | 2.31 | 1 | 0.26 | 11 | 137.62 | 147.42 | 36 | 18 |
| A17 | C ₂₈ H ₂₇ FN ₄ O ₃ S | 518.6 | 7 | 1 | 2.84 | 1 | 0.25 | 11 | 141.46 | 144.26 | 37 | 18 |
| A18 | C ₂₈ H ₂₇ FN ₄ O ₃ S | 518.6 | 8 | 1 | 2.91 | 1 | 0.29 | 8 | 144.41 | 124.64 | 37 | 18 |
| A19 | C ₂₉ H ₂₈ FN ₃ O ₃ S | 517.61 | 7 | 1 | 3.5 | 1 | 0.31 | 10 | 142.15 | 121.4 | 37 | 18 |
| A20 | C ₂₉ H ₂₂ FN ₃ O ₃ S | 511.57 | 7 | 1 | 3.56 | 1 | 0.1 | 8 | 141.82 | 121.4 | 37 | 24 |
| A21 | C ₂₈ H ₂₇ FN ₄ O ₃ S | 518.6 | 8 | 1 | 2.5 | 1 | 0.29 | 10 | 140.23 | 136.42 | 37 | 18 |
| B1 | C ₂₈ H ₂₅ N ₅ O ₄ S | 527.59 | 7 | 1 | 2.22 | 1 | 0.18 | 9 | 146.21 | 148.19 | 38 | 23 |
| B2 | C ₂₈ H ₃₀ N ₄ O ₄ S | 518.63 | 8 | 2 | 1.62 | 1 | 0.29 | 12 | 144.15 | 156.65 | 37 | 18 |
| B3 | C ₂₉ H ₃₀ N ₄ O ₄ S | 530.64 | 8 | 1 | 1.81 | 1 | 0.31 | 11 | 146.8 | 145.65 | 38 | 18 |
| B4 | C ₂₉ H ₃₃ N ₅ O ₃ S | 531.67 | 8 | 2 | 1.81 | 1 | 0.31 | 12 | 150.64 | 148.45 | 38 | 18 |
| B5 | C ₂₉ H ₃₀ N ₄ O ₄ S | 530.64 | 8 | 1 | 1.81 | 1 | 0.31 | 11 | 146.8 | 145.65 | 38 | 18 |
| B6 | C ₂₉ H ₂₈ N ₄ O ₄ S | 528.62 | 7 | 1 | 2.15 | 1 | 0.28 | 10 | 149.89 | 139.5 | 38 | 18 |
| B7 | C ₂₉ H ₂₉ FN ₄ O ₃ S | 532.63 | 8 | 1 | 2.7 | 1 | 0.31 | 10 | 149.78 | 122.43 | 38 | 18 |
| B8 | C ₂₈ H ₃₀ N ₄ O ₄ S | 518.63 | 8 | 2 | 1.62 | 1 | 0.29 | 12 | 144.15 | 156.65 | 37 | 18 |
| B9 | C ₂₈ H ₂₈ N ₅ O ₄ S | 530.62 | 9 | 2 | 1.65 | 1 | 0.29 | 9 | 151.8 | 142.66 | 38 | 18 |
| B10 | C ₃₀ H ₃₁ N ₃ O ₄ S | 529.65 | 7 | 1 | 2.8 | 1 | 0.33 | 11 | 148.68 | 130.63 | 38 | 18 |
| B11 | C ₂₈ H ₂₇ FN ₅ O ₃ S | 532.61 | 9 | 1 | 2.53 | 1 | 0.29 | 9 | 150.69 | 122.43 | 38 | 18 |
| B12 | C ₂₉ H ₃₂ N ₄ O ₄ S | 532.65 | 8 | 2 | 1.81 | 1 | 0.31 | 12 | 149 | 156.65 | 38 | 18 |
| B13 | C ₂₈ H ₂₈ N ₄ O ₄ S | 516.61 | 7 | 1 | 1.95 | 1 | 0.25 | 12 | 143.19 | 153.49 | 37 | 18 |
| B14 | C ₂₈ H ₂₈ N ₄ O ₅ S | 532.61 | 8 | 1 | 1.18 | 1 | 0.25 | 13 | 144.37 | 148.73 | 38 | 18 |
| B15 | C ₃₀ H ₃₂ N ₄ O ₃ S | 528.67 | 7 | 1 | 2.8 | 1 | 0.33 | 11 | 150.53 | 136.42 | 38 | 18 |
| B16 | C ₂₈ H ₃₀ N ₄ O ₄ S | 518.63 | 8 | 1 | 1.62 | 1 | 0.29 | 12 | 144.07 | 145.65 | 37 | 18 |
| B17 | C ₂₈ H ₂₉ N ₅ O ₃ S | 515.63 | 8 | 2 | 1.62 | 1 | 0.29 | 10 | 147.63 | 148.45 | 37 | 18 |
| B18 | C ₃₀ H ₃₁ N ₃ O ₄ S | 529.65 | 7 | 1 | 2.8 | 1 | 0.33 | 10 | 148.98 | 130.63 | 38 | 18 |
| B19 | C ₂₉ H ₃₀ N ₄ O ₄ S | 530.64 | 7 | 1 | 2.15 | 1 | 0.28 | 12 | 148.09 | 139.5 | 38 | 18 |
| B20 | C ₂₈ H ₂₈ N ₅ O ₄ S | 530.62 | 9 | 2 | 1.65 | 1 | 0.29 | 10 | 151.8 | 142.66 | 38 | 18 |
| B21 | C ₃₀ H ₃₂ N ₄ O ₃ S | 528.67 | 7 | 1 | 2.8 | 1 | 0.33 | 10 | 154.5 | 122.43 | 38 | 18 |
| B22 | C ₂₇ H ₂₅ FN ₅ O ₃ S | 518.58 | 9 | 1 | 2.33 | 1 | 0.26 | 9 | 145.88 | 122.43 | 37 | 18 |
| B23 | C ₃₀ H ₃₁ N ₃ O ₄ S | 529.65 | 7 | 1 | 2.8 | 1 | 0.33 | 12 | 148.68 | 130.63 | 38 | 18 |
| B24 | C ₂₉ H ₂₉ N ₃ O ₄ S | 515.62 | 7 | 1 | 2.6 | 1 | 0.31 | 10 | 144.14 | 130.63 | 37 | 18 |

MW: Molecular weight; HBA: H-bond acceptors; HBD: H-bond donors; FCsp³: Fraction Csp³; RB: Rotatable bonds; MR: Molar refractivity; HA: Heavy atoms; AHA: Aromatic heavy atoms.

B1 remained comparable to that of the ligand with the highest binding free energy (ΔG).

3.4. Prediction of ADME properties and toxicity analysis

The evaluation of physicochemical parameters is crucial in assessing the potential of ligands to elicit therapeutic or pharmacological effects. The ADME properties of ligands with docking scores from -11 to -10 kcal/mol from series A and B, as predicted using SwissADME, are reported in Tables 4–6.

Lipinski's rule of 5 provides the criteria for estimating physicochemical properties crucial for the optimum absorption of an orally administered drug. All the tested ligands follow three parameters out of four as defined by Lipinski in Lipinski's rule of 5 [62]. The test ligands should have less than 10 hydrogen bond acceptors, 5 hydrogen bond donors, and MLogP value of less than 4.15 as a lipophilicity threshold. The designed compounds showed molecular weight alert but despite being higher, the molecular weight is still comparable to the specified limit i.e., 500 g/mol. For eg. The designed compound A13 and B24 showed molecular weight of 502.6 g/mol and 515.62 from series A and

Table 5

Lipophilicity profile, solubility profile and pharmacokinetics properties of ligands with best 45 docking scores targeting LSD1.

| Lig. | Solubility Profile | | | Pharmacokinetic Properties | | | | | | | | | |
|------|--------------------|-------|--------------------|----------------------------|--------|-----|--------|------------|---------|--------|--------|--------|-----|
| | LP C. LogP | Log S | Class | GI A | Log Kp | B P | P-gp S | Inhibitors | | | | | |
| | | | | | | | | CYP1A2 | CYP2C19 | CYP2C9 | CYP2D6 | CYP3A4 | |
| A1 | 4.6 | -5.73 | Moderately soluble | Low | -5.93 | No | Yes | No | Yes | Yes | Yes | Yes | Yes |
| A2 | 5.53 | -6.52 | Poorly soluble | Low | -5.2 | No | Yes | No | Yes | Yes | Yes | Yes | Yes |
| A3 | 4.27 | -5.37 | Moderately soluble | Low | -6.58 | No | Yes | No | Yes | Yes | Yes | Yes | Yes |
| A4 | 5.07 | -6.27 | Poorly soluble | Low | -5.7 | No | Yes | No | Yes | Yes | No | Yes | Yes |
| A5 | 5.57 | -6.33 | Poorly soluble | Low | -5.41 | No | Yes | No | Yes | Yes | Yes | No | Yes |
| A6 | 4.15 | -5.42 | Moderately soluble | Low | -6.24 | No | No | Yes | Yes | Yes | No | Yes | Yes |
| A7 | 4.44 | -5.32 | Moderately soluble | Low | -6.34 | No | Yes | No | Yes | Yes | Yes | Yes | Yes |
| A8 | 2.49 | -5.44 | Moderately soluble | Low | -6.52 | No | Yes | No | No | No | No | No | No |
| A9 | 4.16 | -5.57 | Moderately soluble | Low | -6.35 | No | No | Yes | Yes | Yes | No | No | Yes |
| A10 | 4.59 | -5.69 | Moderately soluble | Low | -6.14 | No | Yes | No | Yes | Yes | Yes | Yes | Yes |
| A11 | 4.71 | -5.7 | Moderately soluble | Low | -6.17 | No | Yes | No | Yes | No | No | No | Yes |
| A12 | 4.81 | -5.97 | Moderately soluble | Low | -5.89 | No | Yes | No | Yes | Yes | Yes | No | Yes |
| A13 | 5.27 | -6.23 | Poorly soluble | Low | -5.43 | No | Yes | No | Yes | Yes | Yes | No | Yes |
| A14 | 3.74 | -6.05 | Poorly soluble | Low | -5.8 | No | Yes | No | Yes | Yes | Yes | No | Yes |
| A15 | 4.55 | -5.63 | Moderately soluble | Low | -6.16 | No | Yes | No | Yes | Yes | Yes | Yes | Yes |
| A16 | 4.47 | -5.39 | Moderately soluble | Low | -6.27 | No | Yes | No | Yes | Yes | Yes | Yes | Yes |
| A17 | 5.03 | -6.07 | Poorly soluble | Low | -5.65 | No | No | No | Yes | Yes | No | No | Yes |
| A18 | 4.55 | -6.06 | Poorly soluble | Low | -5.89 | No | Yes | No | Yes | Yes | No | No | Yes |
| A19 | 5.71 | -6.56 | Poorly soluble | Low | -5.16 | No | Yes | No | Yes | Yes | Yes | No | Yes |
| A20 | 5.7 | -7.12 | Poorly soluble | Low | -4.73 | No | No | No | Yes | Yes | No | No | Yes |
| A21 | 4.7 | -5.69 | Moderately soluble | Low | -6.15 | No | Yes | No | Yes | Yes | Yes | Yes | Yes |
| B1 | 4.43 | -6.03 | Poorly soluble | Low | -6.06 | No | Yes | No | No | Yes | No | No | Yes |
| B2 | 4.15 | -5.31 | Moderately soluble | Low | -6.44 | No | Yes | No | Yes | Yes | Yes | Yes | Yes |
| B3 | 4.61 | -5.79 | Moderately soluble | Low | -6.11 | No | Yes | No | Yes | Yes | No | No | Yes |
| B4 | 4.28 | -5.37 | Moderately soluble | Low | -6.53 | No | Yes | No | Yes | No | Yes | Yes | Yes |
| B5 | 4.57 | -5.79 | Moderately soluble | Low | -6.11 | No | Yes | No | Yes | Yes | Yes | No | Yes |
| B6 | 4.47 | -5.88 | Moderately soluble | Low | -6.06 | No | Yes | No | Yes | Yes | Yes | No | Yes |
| B7 | 5.11 | -6.23 | Poorly soluble | Low | -5.72 | No | Yes | No | Yes | Yes | Yes | No | Yes |
| B8 | 4.18 | -5.31 | Moderately soluble | Low | -6.44 | No | Yes | No | Yes | Yes | Yes | Yes | Yes |
| B9 | 2.54 | -5.38 | Moderately soluble | Low | -6.73 | No | Yes | No | No | No | No | No | Yes |
| B10 | 5.45 | -6.52 | Poorly soluble | Low | -5.28 | No | Yes | No | Yes | Yes | No | No | Yes |
| B11 | 3.3 | -6.04 | Poorly soluble | Low | -6.01 | No | Yes | No | Yes | Yes | No | No | Yes |
| B12 | 4.43 | -5.5 | Moderately soluble | Low | -6.39 | No | Yes | No | Yes | No | No | Yes | Yes |
| B13 | 4.44 | -5.55 | Moderately soluble | Low | -6.14 | No | No | No | Yes | Yes | No | No | Yes |
| B14 | 3.95 | -5.28 | Moderately soluble | Low | -6.57 | No | No | Yes | Yes | Yes | Yes | Yes | Yes |
| B15 | 5.3 | -6.33 | Poorly soluble | Low | -5.48 | No | Yes | No | Yes | Yes | No | No | Yes |
| B16 | 4.34 | -5.36 | Moderately soluble | Low | -6.38 | No | Yes | No | Yes | Yes | Yes | Yes | Yes |
| B17 | 3.84 | -5.1 | Moderately soluble | Low | -6.78 | No | Yes | No | Yes | Yes | Yes | Yes | Yes |
| B18 | 5.33 | -6.56 | Poorly soluble | Low | -5.31 | No | Yes | No | Yes | Yes | No | No | Yes |
| B19 | 4.8 | -6.07 | Poorly soluble | Low | -5.73 | No | No | No | Yes | Yes | Yes | No | Yes |
| B20 | 2.39 | -5.16 | Moderately soluble | Low | -6.9 | No | Yes | No | Yes | Yes | Yes | No | Yes |
| B21 | 5.25 | -6.61 | Poorly soluble | Low | -5.24 | No | Yes | No | Yes | Yes | Yes | No | Yes |
| B22 | 2.96 | -5.69 | Moderately soluble | Low | -6.23 | No | Yes | No | Yes | Yes | Yes | No | Yes |
| B23 | 5.47 | -6.53 | Poorly soluble | Low | -5.19 | No | Yes | No | Yes | Yes | Yes | No | Yes |
| B24 | 5.02 | -6.26 | Poorly soluble | Low | -5.48 | No | Yes | No | Yes | Yes | Yes | No | Yes |

LP: Lipophilicity profile; C. LogP: Consensus log Po/w; GI A: GI absorption; BP: BBB permeation; P-gp S: P-gp substrate.

B, respectively.

In the context of ligand bioavailability through oral administration, various physicochemical properties of the ligands must be carefully considered. Notably, the count of rotatable bonds, fraction Csp³, molar refractivity and topological polar surface area (TPSA) are of utmost importance in determining the ligand's potential bioavailability. The saturation of ligands, quantified by the ratio of sp³ hybridized carbons to the total carbon count (Fraction Csp³), should not be less than 0.25 to ensure optimal bioavailability. Similarly, the presence of rotatable bonds, indicative of the ligand flexibility, should be limited to no more than 9. Furthermore, the molar refractivity value is optimal when falling within the range of 40–130. In addition, the ligand's TPSA must lie within 20 and 130 Å² to exhibit significant polarity.

Additionally, the number of aromatic heavy atoms and heavy atoms should fall in the array of 12–14 and 18–22, respectively. The results presented in Table 4 reveal that, while most test compounds except A6, A9, A20 and B1, meet the specified norms for Fraction Csp³ most of the test compounds were within the rotatable bonds and TPSA limits. None of the test compounds adhere to the specified limits for molar refractivity, aromatic heavy atoms, and heavy atoms.

Table 5 (below) illustrates the ligands' lipophilicity profile, solubility profile, and pharmacokinetic properties (GI absorption, skin permeation, BBB permeation, glycoprotein permeability, and cytochrome inhibition).

The characteristic of a chemical substance that dissolves in fats, oils, lipids, or non-polar solvents like toluene and hexane is known as lipophilicity. The partition coefficient between octanol and water (Log P o/w) is a crucial physicochemical parameter in drug development, serving as a mathematical descriptor for lipophilicity. SwissADME determines the compound's lipophilicity using five available predictive models. An overall image, as anticipated by the average of all five models, is provided by the consensus log P value displayed in Table 5. All the compounds showed a reasonable level of lipophilicity (not more than 6), necessary for facilitating interactions between the drug and the membrane receptors.

The solubility profile shows the findings of a water solubility assay, which is crucial for determining the absorption potential of a parenterally administered medicine. Table 5 lists the predicted solubility obtained via the SwissADME server. To ensure proper solubility, it is imperative that the drug's log S value does not exceed -6. The obtained

Table 6

Drug-likeness, bioavailability score, PAINS and synthetic accessibility of ligands with best 45 docking scores targeting LSD1.

| Lig. | Ghose Violations | Veber Violations | Egan Violations | Muegge Violations | BS | PN | Brenk Alerts | SA |
|------|-------------------------------|-------------------------|----------------------------|-------------------|------|----|-----------------------------|------|
| A1 | 2 (MW>480, MR>130) | 0 | 0 | 0 | 0.55 | 0 | 2 (Acyclic: C=C-O, M.A.: 1) | 4.37 |
| A2 | 3 (MW>480, WLOGP>5.6, MR>130) | 0 | 1 (WLOGP>5.88) | 1 (XLOGP3>5) | 0.55 | 0 | 1 (M A.: 1) | 4.41 |
| A3 | 2 (MW>480, MR>130) | 0 | 1 (TPSA>131.6) | 0 | 0.55 | 0 | 1 (M A.: 1) | 4.74 |
| A4 | 3 (MW>480, WLOGP>5.6, MR>130) | 1 (TPSA>140) | 2 (WLOGP>5.88, TPSA>131.6) | 1 (XLOGP3>5) | 0.55 | 0 | 1 (M A.: 1) | 4.64 |
| A5 | 3 (MW>480, WLOGP>5.6, MR>130) | 0 | 1 (WLOGP>5.88) | 1 (XLOGP3>5) | 0.55 | 0 | 1 (M A.: 1) | 4.43 |
| A6 | 2 (MW>480, MR>130) | 1 (Rotors>10) | 1 (TPSA>131.6) | 0 | 0.55 | 0 | 2 (Acyclic: C=C-O, M.A.: 1) | 3.78 |
| A7 | 2 (MW>480, MR>130) | 1 (Rotors>10) | 1 (TPSA>131.6) | 0 | 0.55 | 0 | 1 (M A.: 1) | 4.4 |
| A8 | 2 (MW>480, MR>130) | 0 | 1 (TPSA>131.6) | 0 | 0.55 | 0 | 1 (M A.: 1) | 4.65 |
| A9 | 2 (MW>480, MR>130) | 0 | 1 (TPSA>131.6) | 0 | 0.55 | 0 | 1 (M A.: 1) | 3.9 |
| A10 | 3 (MW>480, WLOGP>5.6, MR>130) | 0 | 1 (WLOGP>5.88) | 0 | 0.55 | 0 | 1 (M A.: 1) | 4.06 |
| A11 | 3 (MW>480, WLOGP>5.6, MR>130) | 1 (TPSA>140) | 2 (WLOGP>5.88, TPSA>131.6) | 0 | 0.55 | 0 | 1 (M A.: 1) | 4.72 |
| A12 | 3 (MW>480, WLOGP>5.6, MR>130) | 0 | 0 | 1 (XLOGP3>5) | 0.55 | 0 | 1 (M A.: 1) | 4.23 |
| A13 | 3 (MW>480, WLOGP>5.6, MR>130) | 0 | 1 (WLOGP>5.88) | 1 (XLOGP3>5) | 0.55 | 0 | 1 (M A.: 1) | 4.28 |
| A14 | 2 (MW>480, MR>130) | 0 | 0 | 1 (XLOGP3>5) | 0.55 | 0 | 1 (M A.: 1) | 4.65 |
| A15 | 3 (MW>480, WLOGP>5.6, MR>130) | 1 (Rotors>10) | 1 (WLOGP>5.88) | 0 | 0.55 | 0 | 1 (M A.: 1) | 4.51 |
| A16 | 3 (MW>480, WLOGP>5.6, MR>130) | 2 (Rotors>10, TPSA>140) | 1 (TPSA>131.6) | 0 | 0.55 | 0 | 1 (M A.: 1) | 4.34 |
| A17 | 3 (MW>480, WLOGP>5.6, MR>130) | 2 (Rotors>10, TPSA>140) | 2 (WLOGP>5.88, TPSA>131.6) | 1 (XLOGP3>5) | 0.55 | 0 | 1 (M A.: 1) | 4.35 |
| A18 | 2 (MW>480, MR>130) | 0 | 0 | 1 (XLOGP3>5) | 0.55 | 0 | 1 (M A.: 1) | 4.72 |
| A19 | 3 (MW>480, WLOGP>5.6, MR>130) | 0 | 1 (WLOGP>5.88) | 1 (XLOGP3>5) | 0.55 | 0 | 1 (M A.: 1) | 3.97 |
| A20 | 3 (MW>480, WLOGP>5.6, MR>130) | 0 | 1 (WLOGP>5.88) | 1 (XLOGP3>5) | 0.55 | 0 | 1 (M A.: 1) | 3.84 |
| A21 | 3 (MW>480, WLOGP>5.6, MR>130) | 0 | 2 (WLOGP>5.88, TPSA>131.6) | 0 | 0.55 | 0 | 1 (M A.: 1) | 4.73 |
| B1 | 2 (MW>480, MR>130) | 1 (TPSA>140) | 1 (TPSA>131.6) | 0 | 0.55 | 0 | 1 (M A.: 1) | 4.13 |
| B2 | 2 (MW>480, MR>130) | 2 (Rotors>10, TPSA>140) | 1 (TPSA>131.6) | 1 (TPSA>150) | 0.55 | 0 | 1 (M A.: 1) | 4.45 |
| B3 | 3 (MW>480, WLOGP>5.6, MR>130) | 2 (Rotors>10, TPSA>140) | 1 (TPSA>131.6) | 0 | 0.55 | 0 | 2 (Acyclic: C=C-O, M.A.: 1) | 4.6 |
| B4 | 3 (MW>480, MR>130, Atoms>70) | 2 (Rotors>10, TPSA>140) | 1 (TPSA>131.6) | 0 | 0.55 | 0 | 1 (M A.: 1) | 4.19 |
| B5 | 3 (MW>480, WLOGP>5.6, MR>130) | 2 (Rotors>10, TPSA>140) | 1 (TPSA>131.6) | 0 | 0.55 | 0 | 2 (Acyclic: C=C-O, M.A.: 1) | 4.64 |
| B6 | 2 (MW>480, MR>130) | 0 | 1 (TPSA>131.6) | 0 | 0.55 | 0 | 1 (M A.: 1) | 4.36 |
| B7 | 3 (MW>480, WLOGP>5.6, MR>130) | 0 | 1 (WLOGP>5.88) | 1 (XLOGP3>5) | 0.55 | 0 | 1 (M A.: 1) | 4.48 |
| B8 | 2 (MW>480, MR>130) | 2 (Rotors>10, TPSA>140) | 1 (TPSA>131.6) | 1 (TPSA>150) | 0.55 | 0 | 1 (M A.: 1) | 4.45 |
| B9 | 2 (MW>480, MR>130) | 1 (TPSA>140) | 1 (TPSA>131.6) | 0 | 0.55 | 0 | 1 (M A.: 1) | 5 |
| B10 | 3 (MW>480, WLOGP>5.6, MR>130) | 1 (Rotors>10) | 1 (WLOGP>5.88) | 1 (XLOGP3>5) | 0.55 | 0 | 1 (M A.: 1) | 4.57 |
| B11 | 2 (MW>480, MR>130) | 0 | 0 | 0 | 0.55 | 0 | 1 (M A.: 1) | 4.98 |
| B12 | 2 (MW>480, MR>130) | 2 (Rotors>10, TPSA>140) | 1 (TPSA>131.6) | 1 (TPSA>150) | 0.55 | 0 | 1 (M A.: 1) | 4.57 |
| B13 | 3 (MW>480, WLOGP>5.6, MR>130) | 2 (Rotors>10, TPSA>140) | 1 (TPSA>131.6) | 1 (TPSA>150) | 0.55 | 0 | 1 (M A.: 1) | 3.91 |
| B14 | 2 (MW>480, MR>130) | 2 (Rotors>10, TPSA>140) | 1 (TPSA>131.6) | 0 | 0.55 | 0 | 1 (M A.: 1) | 4.03 |
| B15 | 3 (MW>480, WLOGP>5.6, MR>130) | 1 (Rotors>10) | 2 (WLOGP>5.88, TPSA>131.6) | 1 (XLOGP3>5) | 0.55 | 0 | 1 (M A.: 1) | 4.57 |
| B16 | 2 (MW>480, MR>130) | 2 (Rotors>10, TPSA>140) | 1 (TPSA>131.6) | 0 | 0.55 | 0 | 1 (M A.: 1) | 4.52 |
| B17 | 2 (MW>480, MR>130) | 2 (Rotors>10, TPSA>140) | 1 (TPSA>131.6) | 0 | 0.55 | 0 | 1 (M A.: 1) | 4 |
| B18 | 3 (MW>480, WLOGP>5.6, MR>130) | 0 | 1 (WLOGP>5.88) | 1 (XLOGP3>5) | 0.55 | 0 | 1 (M A.: 1) | 4.85 |
| B19 | 3 (MW>480, WLOGP>5.6, MR>130) | 1 (Rotors>10) | 1 (TPSA>131.6) | 1 (XLOGP3>5) | 0.55 | 0 | 1 (M A.: 1) | 4.07 |
| B20 | 2 (MW>480, MR>130) | 1 (TPSA>140) | 1 (TPSA>131.6) | 0 | 0.55 | 0 | 1 (M A.: 1) | 4.81 |
| B21 | 3 (MW>480, WLOGP>5.6, MR>130) | 0 | 1 (WLOGP>5.88) | 1 (XLOGP3>5) | 0.55 | 0 | 1 (M A.: 1) | 4.88 |

(continued on next page)

Table 6 (continued)

| Lig. | Ghose Violations | Veber Violations | Egan Violations | Muegge Violations | BS | PN | Brenk Alerts | SA |
|------|-------------------------------|------------------|-----------------|-------------------|------|----|--------------|------|
| B22 | 2 (MW>480, MR>130) | 0 | 0 | 0 | 0.55 | 0 | 1 (M A.: 1) | 4.69 |
| B23 | 3 (MW>480, WLOGP>5.6, MR>130) | 1 (Rotors>10) | 1 (WLOGP>5.88) | 1 (XLOGP3>5) | 0.55 | 0 | 1 (M A.: 1) | 4.09 |
| B24 | 3 (MW>480, WLOGP>5.6, MR>130) | 0 | 1 (WLOGP>5.88) | 1 (XLOGP3>5) | 0.55 | 0 | 1 (M A.: 1) | 4.71 |

MW: Molecular weight; MR: Molar refractivity; BS: Bioavailability score; PN: PAINS; MA: Michael acceptor; SA: Synthetic accessibility.

results suggest that most of the test ligands exhibit modest solubility. Only ligand A20 exhibited a log S value of -7.12 , while all other ligands displayed log S values either below -6 or close to -6 .

The pharmacokinetic properties play a crucial role in governing the behaviour of medications within the human body. Both human gastrointestinal absorption (GI absorption) and blood-brain barrier permeation (BBB permeation) are essential factors as they determine the ability of medications to reach their intended targets for localised effects. The permeation results of test ligands showed low gastrointestinal permeation and no blood-brain barrier permeation. Another critical parameter is skin permeation (Log Kp), with a more negative value representing higher skin permeation. The test ligands demonstrated Log Kp values ranging from -6 to -4 . Additionally, the glycoprotein permeability (P-gp) protein acts as a protective barrier for the central nervous system, preventing the entry of potentially harmful substances. The predicted analysis suggests that most ligands are P-gp substrates except the A6, A9, A17, A20, B13, B14 and B19 ligands.

The cytochromes help in the clearance of a drug through biotransformation, thereby preventing the toxic effects of drug accumulation. SwissADME's therapeutic models include the key isoforms CYP1A2, CYP2C1, CYP2C9, CYP2C19, CYP2D6, and CYP3A4. Inhibition of these cytochromes leads to decreased drug clearance and increased drug accumulation, subsequently resulting in various adverse effects on the body. The results presented in Table 5 indicate that the tested ligands elicited varied responses towards different cytochromes.

The assessment of drug-likeness violations according to the Ghose, Veber, Egan and Muegge rules for the test ligands is depicted in Table 6. The bioavailability scores, which range from 0 to 1, were uniformly recorded as 0.55 for all test ligands, indicating their ability to enter systemic circulation. The Pan-assay interference compounds (PAINS) are the casual or interfering molecules that distort assay results. None of the test ligands exhibited any PAINS interference molecules affecting the assay. When tested against the Brenk filter, all the test ligands displayed one common violation with 1 alert, *i.e.* 1 Michael acceptor, except ligands A1, A6, B3 and B5. These ligands showed another alert for the acyclic (C=C-O) moiety. As defined on a scale of 1 (very easy) to 10 (very difficult) [67], the synthetic accessibility of all tested ligands falls within a range of 3–5, indicating an ease of synthesis.

The toxicity assessment results suggest that none of the 45 test ligands exhibited mutagenic or tumorigenic properties. Regarding reproductive effects, all tested ligands, except B9 and B11, showed no adverse impacts on the reproductive system. However, ligands B9 and B11 pose a medium risk in terms of reproductive effects. Additionally, except for A1 and A6, all test ligands were non-irritating. A1 and A6 were classified as medium-risk irritants, while A15, B2, and B16 were identified as high-risk irritants (Table 7).

The results of physicochemical properties assessments reveal that in series A, test compounds A1, A6, A7, A13 and A16 demonstrate superior characteristics compared to the other tested compounds. These five compounds have molecular weights below 510 g/mol, approximating the molecular weight stipulated by Lipinski. Except for the A6 ligand, all these compounds fall within the specified fraction Csp^3 range. While their solubility varies, all compounds, except A13, exhibit moderate solubility, with A13 classified as poorly soluble. Despite this, the Log S value of A13 is close to -6 . Furthermore, all five compounds, except for

Table 7

Toxicity risks assessment of test ligands.

| Lig. | Mutagenic | Tumorigenic | Irritant | Reproductive Effect |
|------|-----------|-------------|-------------|---------------------|
| A1 | No | No | Medium Risk | No |
| A2 | No | No | No | No |
| A3 | No | No | No | No |
| A4 | No | No | No | No |
| A5 | No | No | No | No |
| A6 | No | No | Medium Risk | No |
| A7 | No | No | No | No |
| A8 | No | No | No | No |
| A9 | No | No | No | No |
| A10 | No | No | No | No |
| A11 | No | No | No | No |
| A12 | No | No | No | No |
| A13 | No | No | No | No |
| A14 | No | No | No | No |
| A15 | No | No | High Risk | No |
| A16 | No | No | No | No |
| A17 | No | No | No | No |
| A18 | No | No | No | No |
| A19 | No | No | No | No |
| A20 | No | No | No | No |
| A21 | No | No | No | No |
| B1 | No | No | No | No |
| B2 | No | No | High Risk | No |
| B3 | No | No | No | No |
| B4 | No | No | No | No |
| B5 | No | No | No | No |
| B6 | No | No | No | No |
| B7 | No | No | No | No |
| B8 | No | No | No | No |
| B9 | No | No | No | Medium Risk |
| B10 | No | No | No | No |
| B11 | No | No | No | Medium Risk |
| B12 | No | No | No | No |
| B13 | No | No | No | No |
| B14 | No | No | No | No |
| B15 | No | No | No | No |
| B16 | No | No | High Risk | No |
| B17 | No | No | No | No |
| B18 | No | No | No | No |
| B19 | No | No | No | No |
| B20 | No | No | No | No |
| B21 | No | No | No | No |
| B22 | No | No | No | No |
| B23 | No | No | No | No |
| B24 | No | No | No | No |

A6, demonstrate impermeability to the blood-brain-barrier and are identified as P-glycoprotein substrates. Significantly, none of these compounds trigger PAINS alerts. Among the five, A1 stands out as the most promising, as it is the only compound with zero violations of Veber, Egan, and Muegge rules within this subset.

The compounds that were screened from series B were B1, B2, B8, B13, B16, B17, B22 and B24. The reason being the lesser molecular weight than the other compounds of series B (Table 1). These eight screened compounds have no permeability to BBB and exhibited 0 PAINS alert and had a bioavailability score of 0.55. Except for compound B13, all compounds were identified as P-glycoprotein substrates. Despite TPSA violations, compound B1 emerged as the best compound from series B due to its drug-likeness, attributed to its non-inhibitory

properties towards the cytochromes, CYP1A2, CYP2C19, and CYP2D6 involved in the detoxification of the body. While the drug's solubility can be adjusted, inhibiting these cytochromes would significantly impact its metabolism.

3.5. MD simulation study

The MD simulation is a method for investigating the atomic and molecular motions of protein-ligand complexes, and enables the assessment of the protein-ligand complex's stability and validates docking results. Our study involved simulating the LIGA1-2DW4 and LIGB1-2DW4 complexes for 400 ns to assess the complex's consistency and, to support the docking findings. The Root Mean Square Deviation (RMSD) value of a protein-ligand complex quantifies the extent of deviation of a particular molecular structure from a reference spatial

environment. The protein RMSD measures the fluctuations of carbon alpha atoms within the protein. The RMSD of protein LSD1, when bound with LIGA1, is depicted by the green colour in Fig. 5A, initially showing minor fluctuations in the range of 3–8 Å up to the timeframe of 130ns. Subsequently, from 130 to 220ns, the fluctuations increased to 9–13 Å, indicating instability of the complex up to 220ns. However, after this point, the complex stabilized and remained stable throughout the remaining simulation.

The protein RMSD with LIGB1 bounded is represented by yellow colour in Fig. 5A. Throughout the simulation, the complex exhibited minimal fluctuations until the 100ns mark, after which it achieved stability and maintained this state for the duration of the simulation.

In Fig. 5B the fluctuations of both the ligands with respect protein from initial to final time frame of simulation is represented by green and yellow colour for LIGA1 and LIGB1, respectively. The plot of LIGA1

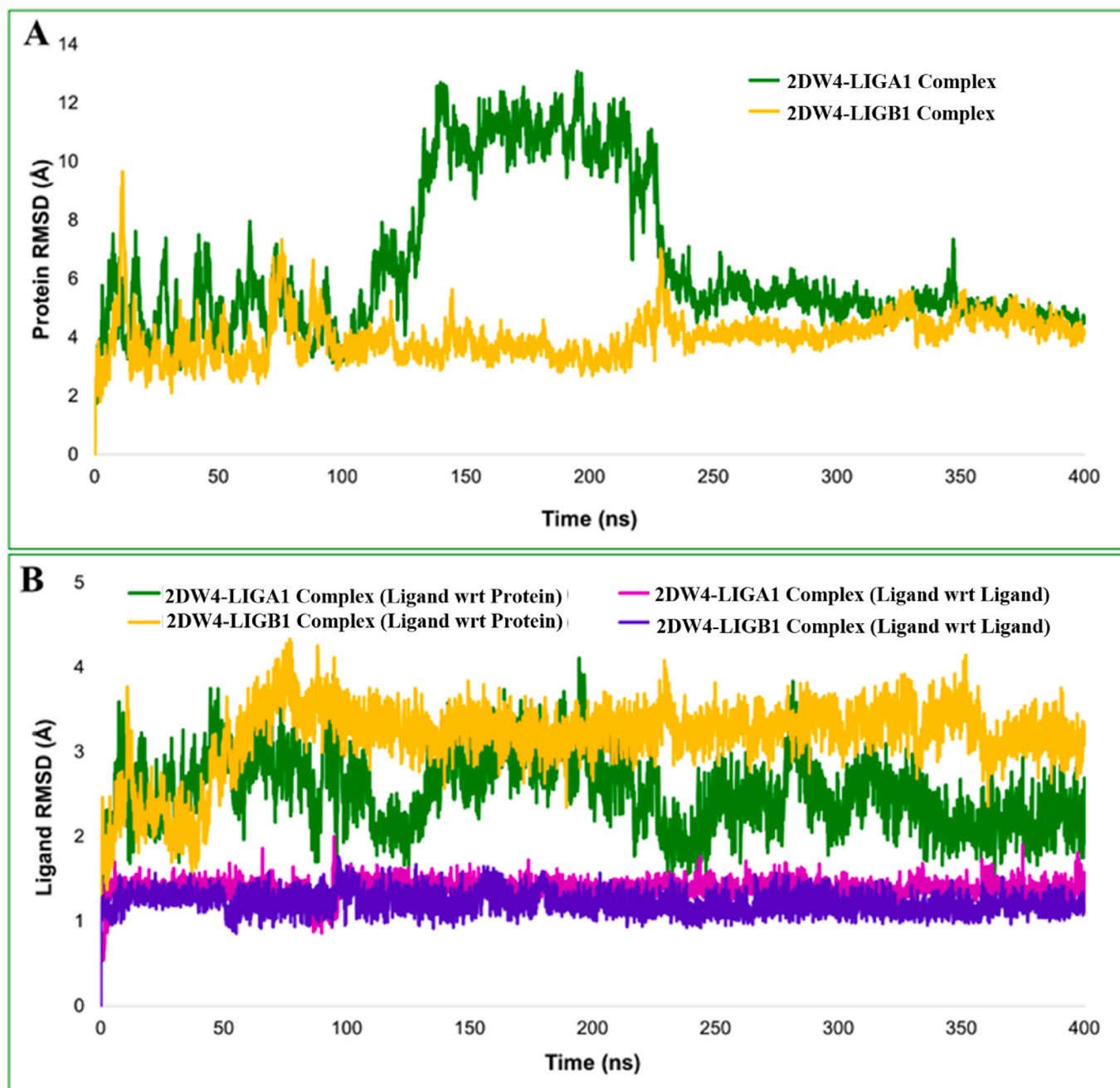


Fig. 5. A: Fluctuations of Protein RMSD and B: Ligand RMSD of the LIGA1-2DW4 and the LIGB1-2DW4 complex.

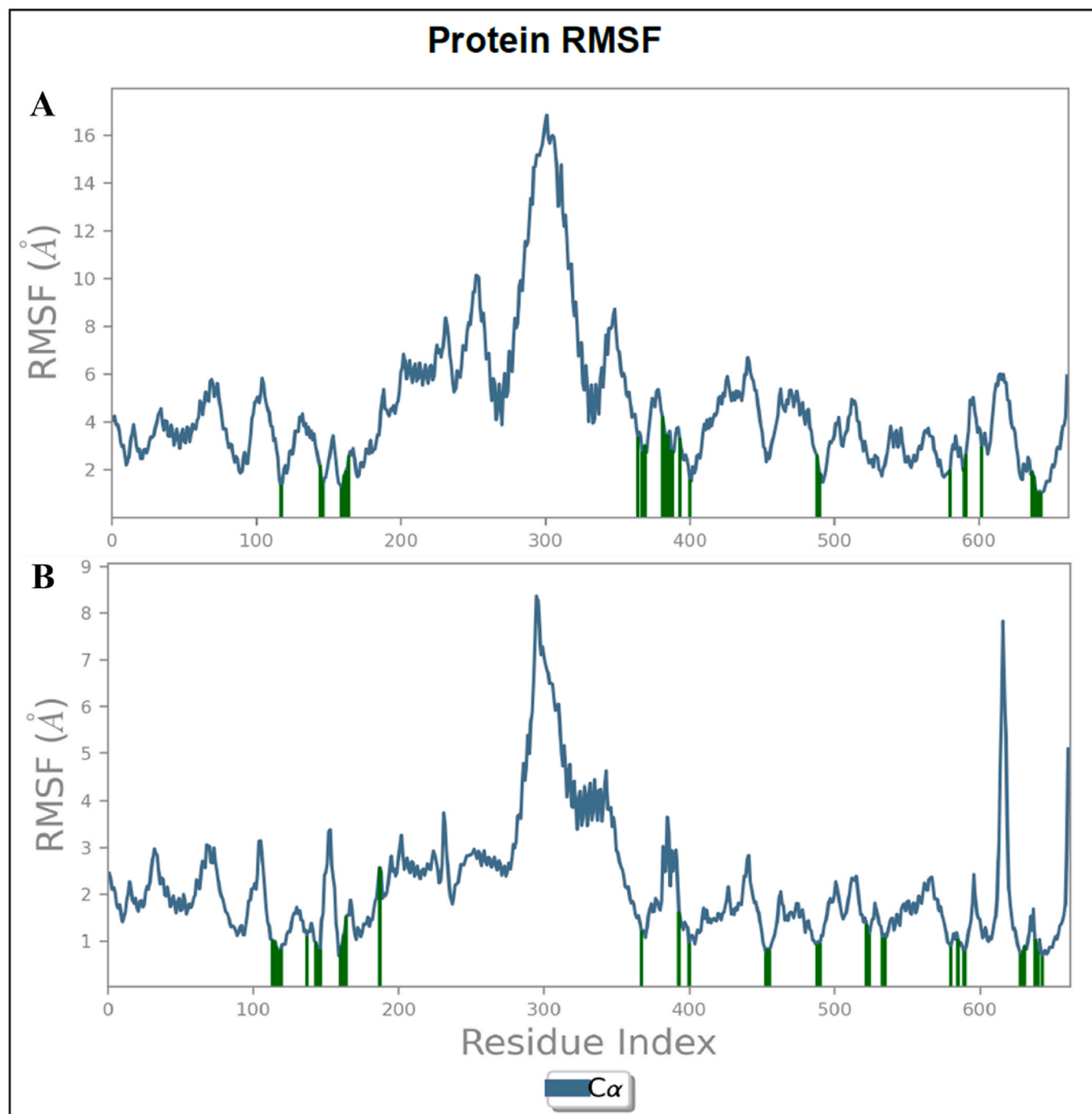


Fig. 6. Protein RMSF of A: LIGA1-2DW4 complex and B: LIGB1-2DW4 complex.

RMSD relative to the protein indicates ligand stabilization after 300ns. In contrast, LIGB1 exhibited initial deviations up to 80ns, followed by stability throughout the simulation.

In Fig. 5B, the RMSD of ligands LIGA1 and LIGB2 in the complex is shown in pink and blue colour, respectively. It depicted deviations of all conformers of the ligands over the simulation timeframe from its initial position at 0ns. The plot shows the stability of both ligands in their initial positions, as the RMSD values range between 1 and 2 Å.

The root mean square fluctuations (RMSF) indicated in Fig. 6 represent the average deviation of the ligand from a reference position over time. The green vertical bars in the figure denote the points at which the ligand comes into contact with the LSD1 protein. In Fig. 6A, the RMSF values for most of the interacting amino acids of LIGA1 are less

than 2 Å, while the corresponding values for LIGB1 in Fig. 6B are less than 1 Å.

Fig. 7 illustrates the distribution of protein-ligand contacts based on different types of bonds observed during the simulation. The histogram bars are colour-coded to represent specific interactions: green for hydrogen bonds, purple for hydrophobic interactions, pink for ionic bonds, and blue for water bridges.

The analysis of the LIGA1-2DW4 complex histogram presented in Fig. 7A indicates that several interactions observed during the initial docking process remained stable throughout the MD simulation. Specifically, the hydrogen bond with GLU559 and the π - π stacking bond with TYR761, as depicted in the 2D interaction diagram of ligand A1 and 2DW4 Complex (Fig. 3), were consistently maintained during the

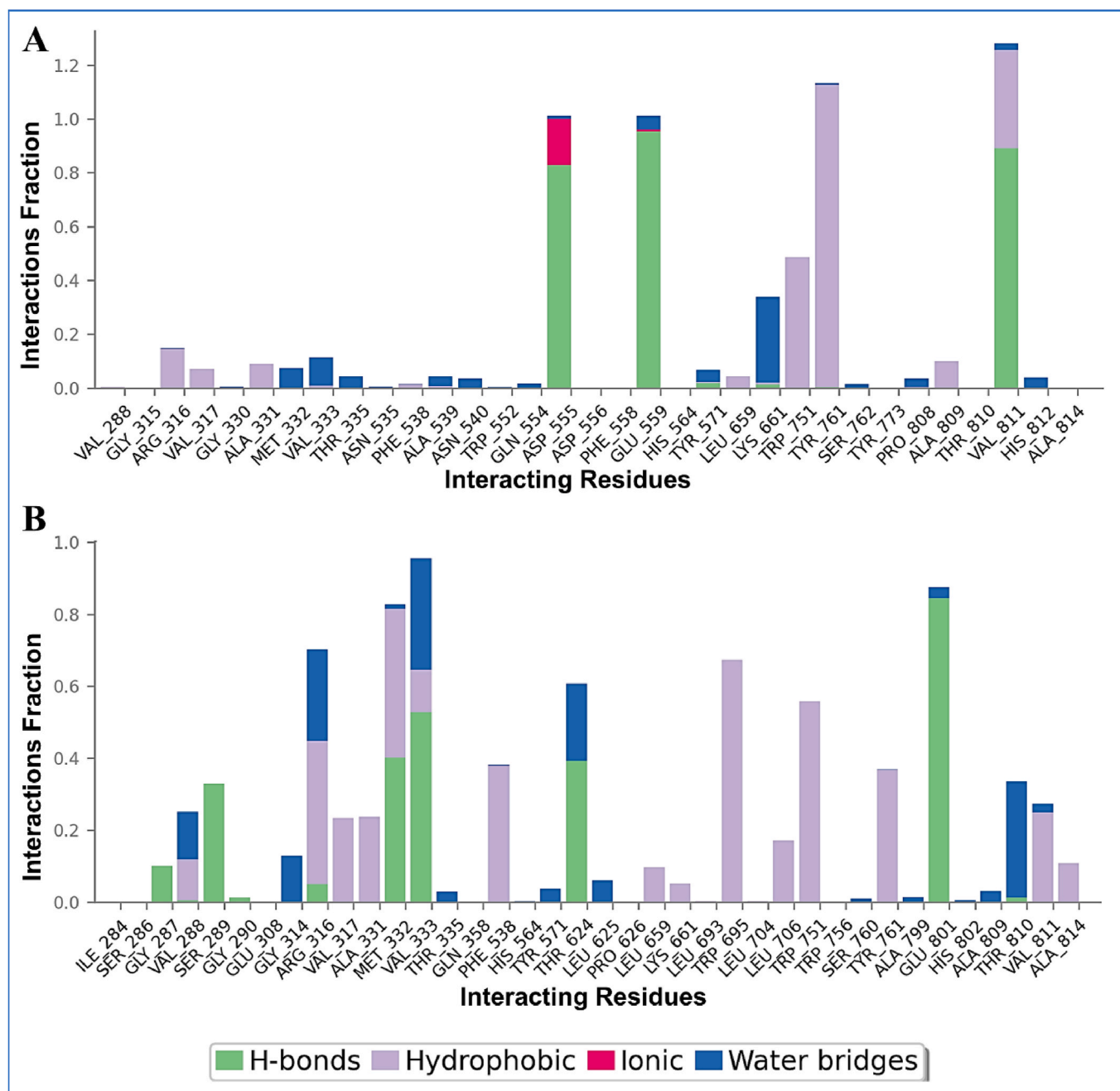


Fig. 7. Protein Ligand contacts histogram of A: LIGA1-2DW4 complex and B: LIGB1-2DW4 complex.

simulation. Furthermore, the MD simulation revealed the presence of four additional hydrogen bonds involving ASP555, TYR571, LYS661, and VAL811. Notably, the histogram illustrates that ligand LIGA1 exhibited significant interactions with ASP555, TYR761, and VAL811 of LSD1.

Fig. 7B displays the protein-ligand contact histogram of the LIGB1-2DW4 complex. The hydrogen bond with ARG316 and π - π stacking bond with TYR 761 (Fig. 4), formed during the docking of the LIGB1-2DW4 complex, remained intact after MD simulation. Additionally, ligand B1 formed ten additional hydrogen bond interactions with the amino-acids GLY287, VAL288, SER289, GLY290, ARG316, MET332, VAL333, THR624, GLU801 and THR810. Furthermore, the LIGB1 displayed prominent interactions with MET332, VAL333 and TYR761, as shown in the histogram (Fig. 7B).

Ligands LIGA1 and LIGB1 exhibited significant interactions with

several critical residues, including TYR761, LYS661, and ARG316, which are known to be critical binding sites for Vafidamstat in their interaction with LSD1, as indicated by Sharba et al. [68]. Additionally, research by Seraj et al. [69] demonstrated that the highly active 5-hydroxypyrazole derivative of this series, when docked with LSD1, display affinities for ARG316, THR810, TYR761, VAL333, VAL288, GLY287, and VAL811, which closely resembles the interactions observed with LIGA1 and LIGB1 in our study. Furthermore, the lead compound described by Ma et al. [42] exhibited interactions with LYS661, VAL288, THR624, ARG316, TYR761, THR810, VAL811, and VAL333. Our designed ligands also demonstrated interactions with these amino acids.

Our study also examined the radius of gyration (rGyr) and the solvent-accessible surface area (SASA) to assess the compactness of the target protein (Fig. 8). The rGyr, which represents the extension of the

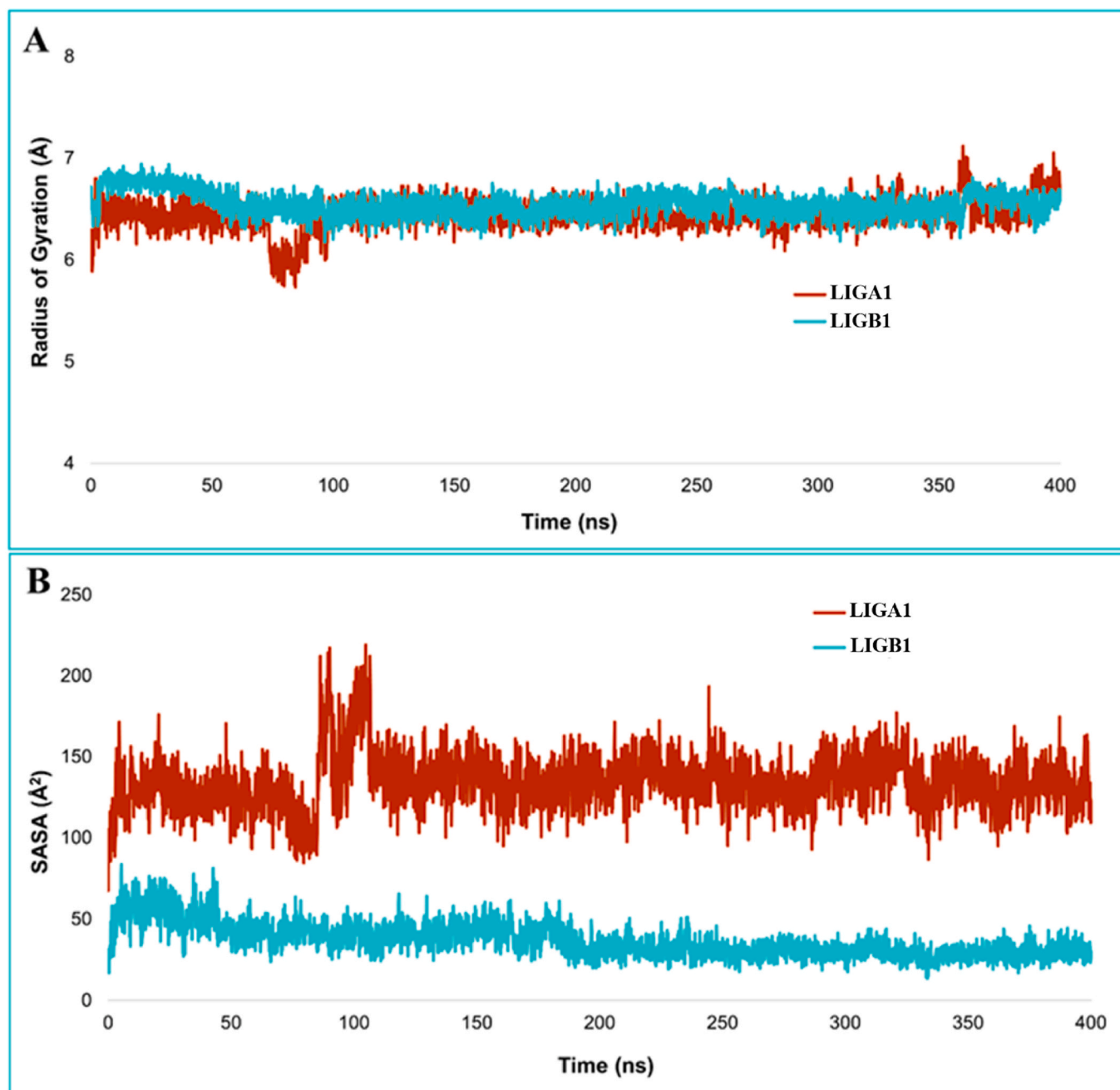


Fig. 8. A: rGyr and B: SASA of the LIGA1-2DW4 complex and the LIGB1-2DW4 complex.

ligands is equivalent to the principal moment of inertia of ligands and was found to range from 5.8 to 7 Å throughout the simulation for both ligands LIGA1 and LIGB1. The rGyr time graph for the LIGB1-protein complex demonstrated stability throughout the simulation. In contrast, the LIGA1-protein complex exhibited minimal fluctuations between 70 and 100 ns. Furthermore, the SASA, which signifies the surface area approachable by a water molecule, was calculated for both ligand complexes. The SASA plots indicated stability in both ligand-protein complexes over the 400 ns simulation period.

4. Conclusion

This manuscript presents a comprehensive analysis of novel cyanopyrimidine pendant chalcone derivatives as potential LSD1 inhibitors. The study employed docking, ADMET, MM/GBSA, and molecular dynamics simulation to elucidate the mechanistic insight. Among the 3668

test ligands (1834 from each series A and B), most exhibited significant docking scores with the LSD1 protein. Notably, ligands A1 and B1, from series A and B, respectively, demonstrated the highest docking scores. Furthermore, the MM-GBSA binding energy of ligands A1 and B1 was found to be -71.97 and -91.03 kcal/mol, respectively. The ADME and toxicity studies also demonstrated favourable responses with respect to various pharmacokinetic and physicochemical parameters.

Additionally, MD simulation of the LIGA1-2DW4 and LIGB1-2DW4 complexes indicated stability within the binding pocket, as evidenced by consistent protein-ligand RMSD and lower RMSF values for most interactions. The protein-ligand contact histogram revealed that fundamental interactions observed during docking were maintained during the simulation, signifying stable ligand-protein interactions.

Furthermore, comparative analysis with known approved drugs and lead compounds documented in the literature indicated notable similarities. Overall, the findings of this computational study suggest that the

lead ligands A1 and B1 form stable complexes with the LSD1 protein, exhibiting potential for further development as anticancer drug candidates. Nonetheless, extensive *in vitro* and *in vivo* preclinical experiments and clinical human trials are imperative to validate their potential for drug development.

5. Future perspectives

This study elucidates the design and evaluation of the novel cyano-pyrimidine pendant chalcone derivatives as LSD1 inhibitors employing virtual screening methodologies such as Docking, ADMET, MM/GBSA, and Molecular Dynamics Simulation. The derivatives demonstrated significantly enhanced potency compared to established pharmaceuticals during virtual screening. We, therefore, intend to synthesize these compounds for subsequent experimental validation, which will encompass *in vitro* testing to substantiate their superior efficacy against cancer cell lines. This phase will be followed by pharmacokinetic and toxicological profiling to ascertain safety and viability. Additionally, *in vivo* studies will evaluate therapeutic efficacy and determine optimal dosing regimens. If the outcomes from the *in vitro* and *in vivo* studies yield favourable results, these novel LSD1 inhibitors may serve as lead candidates for further optimization and clinical development.

CRedit authorship contribution statement

Amisha Gupta: Writing – original draft, Formal analysis, Conceptualization. **Darakhshan Parveen:** Software, Formal analysis. **Faizul Azam:** Software, Formal analysis. **M. Shaquiquzzaman:** Supervision, Resources. **Mymoona Akhter:** Validation, Software. **Mariusz Jaremko:** Writing – review & editing. **Abdul-Hamid Emwas:** Writing – review & editing. **Mohammad Ahmed Khan:** Investigation, Formal analysis. **Suhel Parvez:** Supervision. **Suruchi Khanna:** Formal analysis. **Rituparna Palit:** Writing – review & editing. **Umar Jahangir:** Writing – review & editing. **M. Mumtaz Alam:** Validation, Supervision, Conceptualization.

Declaration of competing interest

The authors declare that they have no known competing financial interests or personal relationships that could have appeared to influence the work reported in this paper.

Acknowledgements

The authors thankfully acknowledge Jamia Hamdard and DST INSPIRE (INSPIRE Code: IF210082), for providing the infrastructure facilities and funds.

References

- P. Bober, M. Alexovič, Z. Tomková, R. Kilič, J. Sabo, RHOA and mDia1 promotes apoptosis of breast cancer cells via a high dose of doxorubicin treatment, *Open Life Sci.* 14 (2019) 619–627.
- Y. Chen, Y. Yang, F. Wang, K. Wan, K. Yamane, Y. Zhang, M. Lei, Crystal structure of human histone lysine-specific demethylase 1 (LSD1), *Proc. Natl. Acad. Sci. USA* 103 (2006) 13956–13961.
- S. Lin, X. Li, Epigenetic therapies and potential drugs for treating human Cancer, *Curr. Drug Targets* 21 (2020) 1068–1083.
- Y. Li, B. Wang, Y. Zheng, H. Kang, A. He, L. Zhao, N. Guo, H. Liu, A. Mardinoglu, M. A.A. Mamun, The multifaceted role of post-translational modifications of LSD1 in cellular processes and disease pathogenesis, *Genes Dis* (2024) 101307.
- Y. Fang, G. Liao, B. Yu, Targeting histone lysine demethylase LSD1/KDM1A as a new avenue for cancer therapy, *Curr. Top. Med. Chem.* 19 (2019) 889–891.
- S. Amente, L. Lania, B. Majello, The histone LSD1 demethylase in stemness and cancer transcription programs, *Biochim. Biophys. Acta (BBA)-Gene Regul. Mech.* 1829 (2013) 981–986.
- A. Janardhan, C. Kathera, A. Darsi, W. Ali, L. He, Y. Yang, L. Luo, Z. Guo, Prominent role of histone lysine demethylases in cancer epigenetics and therapy, *Oncotarget* 9 (2018) 34429.
- F. Sarno, A. Nebbioso, L. Altucci, Histone demethylase inhibitors and their potential in cancer treatment, in: *Histone Modif. Ther.*, Elsevier, 2020, pp. 143–177.
- J.C. Culhane, P.A. Cole, LSD1 and the chemistry of histone demethylation, *Curr. Opin. Chem. Biol.* 11 (2007) 561–568.
- F. Forneris, C. Binda, A. Dall'Aglio, M.W. Fraaije, E. Battaglioli, A. Mattevi, A highly specific mechanism of histone H3-K4 recognition by histone demethylase LSD1, *J. Biol. Chem.* 281 (2006) 35289–35295.
- J. Dong, W. Pervaiz, B. Tayyab, D. Li, L. Kang, H. Zhang, H. Gong, X. Ma, J. Li, C. Agboyibor, A comprehensive comparative study on LSD1 in different cancers and tumor specific LSD1 inhibitors, *Eur. J. Med. Chem.* 240 (2022) 114564.
- S.N. Vasilatos, T.A. Katz, S. Oesterreich, Y. Wan, N.E. Davidson, Y. Huang, Crosstalk between lysine-specific demethylase 1 (LSD1) and histone deacetylases mediates antineoplastic efficacy of HDAC inhibitors in human breast cancer cells, *Carcinogenesis* 34 (2013) 1196–1207.
- S. Sainathan, S. Paul, S. Ramalingam, J. Baranda, S. Anant, A. Dhar, Histone demethylases in cancer, *Curr. Pharmacol. Rep.* 1 (2015) 234–244.
- N. Wang, T. Ma, B. Yu, Targeting epigenetic regulators to overcome drug resistance in cancers, *Signal Transduct. Targeted Ther.* 8 (2023) 69.
- M.E. Neganova, S.G. Klochkov, Y.R. Aleksandrova, G. Aliev, Histone modifications in epigenetic regulation of cancer: perspectives and achieved progress, in: *Semin. Cancer Biol.*, Elsevier, 2022, pp. 452–471.
- S. Konovalov, I. Garcia-Bassets, Analysis of the levels of lysine-specific demethylase 1 (LSD1) mRNA in human ovarian tumors and the effects of chemical LSD1 inhibitors in ovarian cancer cell lines, *J. Ovarian Res.* 6 (2013) 1–15.
- H. Liu, Y. Zhou, H. Chen, J. Wu, S. Ji, L. Shen, S. Wang, H. Liu, Y. Liu, X. Dai, LSD1 in drug discovery: from biological function to clinical application, *Med. Res. Rev.* 44 (2024) 833–866.
- T. Maes, C. Mascaró, D. Rotllant, M.M.P. Lufino, A. Estiarte, N. Guibourt, F. Cavalcanti, C. Griñan-Ferré, M. Pallàs, R. Nadal, Modulation of KDM1A with vafidemstat rescues memory deficit and behavioral alterations, *PLoS One* 15 (2020) e0233468.
- E. Cuyàs, J. Gumuzio, S. Verdura, J. Brunet, J. Bosch-Barrera, B. Martin-Castillo, T. Alarcón, J.A. Encinar, Á.G. Martín, J.A. Menendez, The LSD1 inhibitor iadademstat (ORY-1001) targets SOX2-driven breast cancer stem cells: a potential epigenetic therapy in luminal-B and HER2-positive breast cancer subtypes, *Aging (Albany NY)* 12 (2020) 4794.
- Y. C. Zheng, B. Yu, G. Z. Jiang, X.J. Feng, P.X. He, X. Y. Chu, W. Zhao, H. M. Liu, Irreversible LSD1 inhibitors: application of tranlylcypromine and its derivatives in cancer treatment, *Curr. Top. Med. Chem.* 16 (2016) 2179–2188.
- W. Fiskus, S. Sharma, S. Abhyankar, J. McGuirk, D.J. Bearss, K. Bhalla, Pre-clinical efficacy of combined therapy with LSD1 antagonist SP-2509 and pan-histone deacetylase inhibitor against AML blast progenitor cells, *Blood* 120 (2012) 868.
- G.J. Roboz, K. Yee, A. Verma, G. Borthakur, A. de la Fuente Burguera, G. Sanz, H. P. Mohammad, R.G. Kruger, N.O. Karpinich, G. Ferron-Brady, Phase I trials of the lysine-specific demethylase 1 inhibitor, GSK2879552, as mono- and combination-therapy in relapsed/refractory acute myeloid leukemia or high-risk myelodysplastic syndromes, *Leuk. Lymphoma* 63 (2022) 463–467.
- T. Kanouni, C. Severin, R.W. Cho, N.Y.-Y. Yuen, J. Xu, L. Shi, C. Lai, J.R. Del Rosario, R.K. Stansfield, L.N. Lawton, Discovery of CC-90011: a potent and selective reversible inhibitor of lysine specific demethylase 1 (LSD1), *J. Med. Chem.* 63 (2020) 14522–14529.
- Y. Liang, D. Quenelle, J.L. Vogel, C. Mascaró, A. Ortega, T.M. Kristie, A novel selective LSD1/KDM1A inhibitor epigenetically blocks herpes simplex virus lytic replication and reactivation from latency, *mBio* 4 (2013) 10–1128.
- Cancer, (n.d.). <https://www.who.int/news-room/fact-sheets/detail/cancer> (accessed May 29, 2024).
- N. Abbas, G.S.P. Matada, P.S. Dhiwar, S. Patel, G. Devasahayam, Fused and substituted pyrimidine derivatives as profound anti-cancer agents, *Anti Cancer Agents Med. Chem.* 21 (2021) 861–893.
- D.B. Longley, D.P. Harkin, P.G. Johnston, 5-fluorouracil: mechanisms of action and clinical strategies, *Nat. Rev. Cancer* 3 (2003) 330–338.
- L.M. Nainwal, M. Shaququzzaman, M. Akhter, A. Husain, S. Parvez, S. Tasneem, A. Iqbal, M.M. Alam, Synthesis, and reverse screening of 6-(3, 4, 5-trimethoxyphenyl) pyrimidine-5-carbonitrile derivatives as anticancer agents: Part-II, *J. Heterocycl. Chem.* 59 (2022) 771–788.
- S. Li, X. Qi, Y. Huang, D. Liu, F. Zhou, C. Zhou, Ceritinib (LDK378): a potent alternative to crizotinib for ALK-rearranged non-small-cell lung cancer, *Clin. Lung Cancer* 16 (2015) 86–91.
- H. Kantarjian, E. Jabbour, J. Grimley, P. Kirkpatrick, Dasatinib, *Nat. Rev. Drug Discov.* 5 (2006).
- M. Deininger, E. Buchdunger, B.J. Druker, The development of imatinib as a therapeutic agent for chronic myeloid leukemia, *Blood* 105 (2005) 2640–2653.
- P. Ghia, C. Owen, J.C. Barrientos, P.M. Barr, A.R. Mato, C. Shi, A. Szoke, C. Abbazio, G.S. Krigsfeld, J.A. Burger, Initiating first-line (1L) ibrutinib (Ibr) in patients (pts) with chronic lymphocytic leukemia (CLL) improves overall survival (OS) outcomes to rates approximating an age-matched population of ≥ 65 years, *Blood* 140 (2022) 4159–4161.
- J.M. Fortune, N. Osheroff, Merbarone inhibits the catalytic activity of human topoisomerase II α by blocking DNA cleavage, *J. Biol. Chem.* 273 (1998) 17643–17650.
- J.-Y. Blay, M. von Mehren, Nilotinib: a novel, selective tyrosine kinase inhibitor, in: *Semin. Oncol.*, Elsevier, 2011, pp. 53–59.
- S. Ajayi, H. Becker, H. Reinhardt, M. Engelhardt, R. Zeiser, N. von Bubnoff, R. Wäsch, Ruxolitinib, *Small Mol. Hematol.* 2018, pp. 119–132.
- Y.Y. Syed, Ribociclib: first global approval, *Drugs* 77 (2017) 799–807.

- [37] J.A. Mosow, Methotrexate transport and resistance, *Leuk. Lymphoma* 30 (1998) 215–224.
- [38] Z. Li, L. Ding, Z. Li, Z. Wang, F. Suo, D. Shen, T. Zhao, X. Sun, J. Wang, Y. Liu, Development of the triazole-fused pyrimidine derivatives as highly potent and reversible inhibitors of histone lysine specific demethylase 1 (LSD1/KDM1A), *Acta Pharm. Sin. B* 9 (2019) 794–808.
- [39] N.H. Metwally, M.S. Mohamed, E.A. Ragb, Design, synthesis, anticancer evaluation, molecular docking and cell cycle analysis of 3-methyl-4, 7-dihydropyrazolo [1, 5-a] pyrimidine derivatives as potent histone lysine demethylases (KDM) inhibitors and apoptosis inducers, *Bioorg. Chem.* 88 (2019) 102929.
- [40] S. Wang, Z.-R. Li, F.-Z. Suo, X.-H. Yuan, B. Yu, H.-M. Liu, Synthesis, structure-activity relationship studies and biological characterization of new [1, 2, 4] triazolo [1, 5-a] pyrimidine-based LSD1/KDM1A inhibitors, *Eur. J. Med. Chem.* 167 (2019) 388–401.
- [41] S. Xu, C. Zhou, R. Liu, Q. Zhu, Y. Xu, F. Lan, X. Zha, Optimization of 5-arylidene barbiturates as potent, selective, reversible LSD1 inhibitors for the treatment of acute promyelocytic leukemia, *Bioorg. Med. Chem.* 26 (2018) 4871–4880.
- [42] L. Ma, H. Wang, Y. You, C. Ma, Y. Liu, F. Yang, Y. Zheng, H. Liu, Exploration of 5-cyano-6-phenylpyrimidin derivatives containing an 1,2,3-triazole moiety as potent FAD-based LSD1 inhibitors, *Acta Pharm. Sin. B* 10 (2020) 1658–1668, <https://doi.org/10.1016/j.apsb.2020.02.006>.
- [43] F. Gao, G. Huang, J. Xiao, Chalcone hybrids as potential anticancer agents: current development, mechanism of action, and structure-activity relationship, *Med. Res. Rev.* 40 (2020) 2049–2084.
- [44] E.M. Othman, E.A. Fayed, E.M. Husseiny, H.S. Abulkhair, Apoptosis induction, PARP-1 inhibition, and cell cycle analysis of leukemia cancer cells treated with novel synthetic 1,2,3-triazole-chalcone conjugates, *Bioorg. Chem.* 123 (2022) 105762, <https://doi.org/10.1016/j.bioorg.2022.105762>.
- [45] S. Rahimzadeh Oskuei, S. Mirzaei, M. Reza Jafari-Nik, F. Hadizadeh, F. Eivsand, F. Mosaffa, R. Ghodsi, Design, synthesis and biological evaluation of novel imidazole-chalcone derivatives as potential anticancer agents and tubulin polymerization inhibitors, *Bioorg. Chem.* 112 (2021) 104904, <https://doi.org/10.1016/j.bioorg.2021.104904>.
- [46] Y. Luo, W. Wu, D. Zha, W. Zhou, C. Wang, J. Huang, S. Chen, L. Yu, Y. Li, Q. Huang, J. Zhang, C. Zhang, Synthesis and biological evaluation of novel ligustrazine-chalcone derivatives as potential anti-triple negative breast cancer agents, *Bioorg. Med. Chem. Lett.* 47 (2021) 128230, <https://doi.org/10.1016/j.bmcl.2021.128230>.
- [47] E.-B. Yang, K. Zhang, L.Y. Cheng, P. Mack, Butein, a specific protein tyrosine kinase inhibitor, *Biochem. Biophys. Res. Commun.* 245 (1998) 435–438.
- [48] S. Girisa, Q. Saikia, D. Bordoloi, K. Banik, J. Monisha, U.D. Daimary, E. Verma, K. S. Ahn, A.B. Kunnumakkara, Xanthohumol from Hop: hope for cancer prevention and treatment, *IUBMB Life* 73 (2021) 1016–1044, <https://doi.org/10.1002/iub.2522>.
- [49] F. Peng, Q. Du, C. Peng, N. Wang, H. Tang, X. Xie, J. Shen, J. Chen, A review: the pharmacology of isoliquiritigenin, *Phyther. Res.* 29 (2015) 969–977.
- [50] M.-T. Li, L. Xie, H.-M. Jiang, Q. Huang, R.-S. Tong, X. Li, X. Xie, H.-M. Liu, Role of licochalcone A in potential pharmacological therapy: a review, *Front. Pharmacol.* 13 (2022) 878776.
- [51] B. Ngameni, K. Cedric, A.T. Mbaveng, M. Erdogan, I. Simo, V. Kuete, A. Daştan, Design, synthesis, characterization, and anticancer activity of a novel series of O-substituted chalcone derivatives, *Bioorg. Med. Chem. Lett.* 35 (2021) 127827.
- [52] D. Srilaxmi, R. Sreenivasulu, K.K. Mak, M.R. Pichika, S.S. Jadav, M.J. Ahsan, M.V. B. Rao, Design, synthesis, anticancer evaluation and molecular docking studies of chalcone linked pyrido[4,3-b]pyrazin-5(6H)-one derivatives, *J. Mol. Struct.* 1229 (2021) 129851, <https://doi.org/10.1016/j.molstruc.2020.129851>.
- [53] S. Wang, L.-J. Zhao, Y.-C. Zheng, D.-D. Shen, E.-F. Miao, X.-P. Qiao, L.-J. Zhao, Y. Liu, R. Huang, B. Yu, Design, synthesis and biological evaluation of [1, 2, 4] triazolo [1, 5-a] pyrimidines as potent lysine specific demethylase 1 (LSD1/KDM1A) inhibitors, *Eur. J. Med. Chem.* 125 (2017) 940–951.
- [54] C. Bagul, G.K. Rao, V.K.K. Makani, J.R. Tamboli, M. Pal-Bhadra, A. Kamal, Synthesis and biological evaluation of chalcone-linked pyrazolo [1, 5-a] pyrimidines as potential anticancer agents, *Medchemcomm* 8 (2017) 1810–1816.
- [55] W. Akhtar, L.M. Nainwal, S.K. Kaushik, M. Akhtar, M. Shaquiquzzaman, F. Almalki, K. Saifullah, A. Marella, M.M. Alam, Methylene-bearing sulfur-containing cyanopyrimidine derivatives for treatment of cancer: Part-II, *Arch. Pharm. (Weinheim)* 353 (2020) e1900333.
- [56] M. Mustafa, J.-Y. Winum, The importance of sulfur-containing motifs in drug design and discovery, *Expert Opin. Drug Discov.* 17 (2022) 501–512.
- [57] F.F. Fleming, L. Yao, P.C. Ravikumar, L. Funk, B.C. Shook, Nitrile-containing pharmaceuticals: efficacious roles of the nitrile pharmacophore, *J. Med. Chem.* 53 (2010) 7902–7917.
- [58] K.A. Sheikh, D. Parveen, M.M. Alam, F. Azam, M.A. Khan, M. Akhter, S. Tasneem, S. Parvez, K. Imtiyaz, M.A. Rizvi, Exploring cyclopropylamine containing cyanopyrimidines as LSD1 inhibitors: design, synthesis, ADMET, MD analysis and anticancer activity profiling, *Bioorg. Chem.* 147 (2024) 107336.
- [59] A.C. Alves, D. Ribeiro, C. Nunes, S. Reis, Biophysics in cancer: the relevance of drug-membrane interaction studies, *Biochim. Biophys. Acta, Biomembr.* 1858 (2016) 2231–2244.
- [60] R.A. Friesner, R.B. Murphy, M.P. Repasky, L.L. Frye, J.R. Greenwood, T.A. Halgren, P.C. Sanschagrin, D.T. Mainz, Extra precision glide: docking and scoring incorporating a model of hydrophobic enclosure for protein–ligand complexes, *J. Med. Chem.* 49 (2006) 6177–6196.
- [61] M.P. Jacobson, D.L. Pincus, C.S. Rapp, T.J.F. Day, B. Honig, D.E. Shaw, R. A. Friesner, A hierarchical approach to all-atom protein loop prediction, *Proteins: Struct., Funct., Bioinf.* 55 (2004) 351–367.
- [62] A. Daina, O. Michielin, V. Zoete, SwissADME: a free web tool to evaluate pharmacokinetics, drug-likeness and medicinal chemistry friendliness of small molecules, *Sci. Rep.* 7 (2017) 42717.
- [63] T. Sander, J. Freys, M. Korff, J.R. Reich, C. Rufener, OSIRIS, an entirely in-house developed drug discovery informatics system, *J. Chem. Inf. Model.* 49 (2) (2009) 232–246, <https://doi.org/10.1021/ci800305f>.
- [64] K.J. Bowers, E. Chow, H. Xu, R.O. Dror, M.P. Eastwood, B.A. Gregersen, J. L. Klepeis, I. Kolossvary, M.A. Moraes, F.D. Sacerdoti, Scalable algorithms for molecular dynamics simulations on commodity clusters, in: *Proc. 2006 ACM/IEEE Conf. Supercomput.*, 2006, pp. 84–es.
- [65] S. Amin, K.A. Sheikh, A. Iqbal, M.A. Khan, M. Shaquiquzzaman, S. Tasneem, S. Khanna, A.K. Najmi, M. Akhter, A. Haque, Synthesis, in-Silico studies and biological evaluation of pyrimidine based thiazolidinedione derivatives as potential anti-diabetic agent, *Bioorg. Chem.* 134 (2023) 106449.
- [66] D. Parveen, A. Das, S. Amin, M.M. Alam, M. Akhter, M. Ahmed Khan, R. Ali, T. Anwer, K.A. Sheikh, F. Azam, Effectiveness of estrogen and its derivatives over dexamethasone in the treatment of COVID-19, *J. Biomol. Struct. Dyn.* (2023) 1–17.
- [67] D. Ranjith, C. Ravikumar, SwissADME predictions of pharmacokinetics and drug-likeness properties of small molecules present in *Ipomoea mauritiana* Jacq, *J. Pharmacogn. Phytochem.* 8 (2019) 2063–2073.
- [68] S. Tasneem, K.A. Sheikh, M. Naematullah, M. Mumtaz Alam, F. Khan, M. Garg, M. Amir, M. Akhter, S. Amin, A. Haque, M. Shaquiquzzaman, Synthesis, biological evaluation and docking studies of methylene bearing cyanopyrimidine derivatives possessing a hydrazone moiety as potent Lysine specific demethylase-1 (LSD1) inhibitors: a promising anticancer agents, *Bioorg. Chem.* 126 (2022) 105885, <https://doi.org/10.1016/j.bioorg.2022.105885>.
- [69] K. Seraj, M. Asadollahi-Baboli, In silico evaluation of 5-hydroxypyrazoles as LSD1 inhibitors based on molecular docking derived descriptors, *J. Mol. Struct.* 1179 (2019) 514–524, <https://doi.org/10.1016/j.molstruc.2018.11.019>.